Final Report Testing of Iron Phosphate LAW Glass (VSL-11R2340-1) April 25, 2011

Rev 0;6/10/11

Final Report Testing of Iron Phosphate LAW Glass (VSL-11R2340-1) April 25, 2011

Rev 0;6/10/11

H. Gan
A. C. Buechele
Z. Feng
C. Wang
C. Viragh
I. L. Pegg
Vitreous State Laboratory
The Catholic University of America

A. A. Kruger
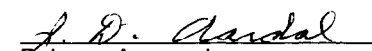Department of Energy - Office of River Protection

I. Joseph
EnergySolutions Federal EPC, Inc.

Office of River Protection

Release Approval   Date

VSL-11R2340-1

Final Report

Testing of Iron Phosphate LAW Glass

prepared by

Hao Gan, Andrew C. Buechele, Zhijian Feng, Chuan Wang, Carol Viragh, and Ian L. Pegg

Vitreous State Laboratory
The Catholic University of America
Washington, DC 20064

and

Innocent Joseph

Energy*Solutions* Federal EPC, Inc.
Columbia, MD

for
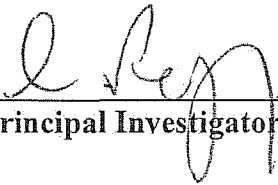
Washington River Protection *Solutions*, LLC

April 25, 2011

Rev. 0; 6/10/11

Completeness of Testing:

This report describes the results of work and testing specified by WRPS. The work and any associated testing followed established quality assurance requirements. The descriptions provided in this test report are an accurate account of both the conduct of the work and the data collected. Results required by the test program are reported. Also reported are any unusual or anomalous occurrences that are different from the starting hypotheses. The test results and this report have been reviewed and verified.

I. L. Pegg: _____ Date: 6-10-11
VSL Program Director/Principal Investigator

I. Joseph: _____ Date: 6/10/11
Energy*Solutions* Sub-Contract Manager

TABLE OF CONTENTS

List of Tables
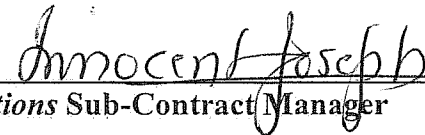
List of Figures

5

List of Abbreviations

ASME	American Society of Mechanical Engineers
CEES	Columbia Energy and Environmental Services
CUA	The Catholic University of America
DOE	Department of Energy
DSC	Differential Scanning Calorimetry
EDS	Energy Dispersive X-ray Spectroscopy
FeP	Iron Phosphate
IHLW	Immobilized High Level Waste
ILAW	Immobilized Low Activity Waste
INL	Idaho National Laboratory
JHCM	Joule Heated Ceramic Melter
LAW	Low Activity Waste
MS&T	Missouri University of Science and Technology
NIST	National Institute of Standards and Technology
NQA	Nuclear Quality Assurance
ORP	Office of River Protection
PNNL	Pacific Northwest National Laboratory
QARD	Quality Assurance Requirements and Description
SEM	Scanning Electron Microscopy
SRNL	Savannah River National Laboratory
TDD	DOE EM-31 Technology Development & Deployment
US	United States
VSL	Vitreous State Laboratory
WTP	Hanford Tank Waste Treatment and Immobilization Plant
WRPS	Washington River Protection *Solutions*
XRF	X-Ray Fluorescence Spectroscopy

SECTION 1.0
INTRODUCTION

About 50 million gallons of high-level mixed waste is currently stored in underground tanks at The United States Department of Energy's (DOE's) Hanford site in the State of Washington. The Hanford Tank Waste Treatment and Immobilization Plant (WTP) will provide DOE's Office of River Protection (ORP) with a means of treating this waste by vitrification for subsequent disposal. The tank waste will be separated into low- and high-activity waste fractions, which will then be vitrified respectively into Immobilized Low Activity Waste (ILAW) and Immobilized High Level Waste (IHLW) products. The ILAW product will be disposed in an engineered facility on the Hanford site while the IHLW product will likely be directed to a national deep geological disposal facility for high-level nuclear waste. The ILAW and IHLW products must meet a variety of requirements with respect to protection of the environment before they can be accepted for disposal.

For a number of Hanford low activity waste (LAW) streams, sulfur is the main component that limits waste loading in glass. However, for other LAW streams with low sulfate contents, the alkali concentration becomes the waste loading limiting factor. In general, waste loading is limited by sulfur for wastes with a high sulfur-to-sodium ratio, while those with a low sulfur-to-sodium ratio are limited by sodium (or more specifically, total alkali (sodium plus potassium)). Minimizing overall glass volume across the entire LAW inventory, which is clearly of economic benefit, therefore, entails addressing both the sulfur limitation and the alkali limitation, depending on the waste type. Borosilicate glass has been selected as the baseline material to immobilize Hanford LAW. In the baseline borosilicate glasses developed for the WTP [1-3], the maximum Na_2O and SO_3 loadings were limited to about 20 wt% and 0.5 wt%, respectively, resulting in an average Na_2O loading of about 13 wt% across all of the Hanford LAW streams. Subsequent work by the Vitreous State Laboratory (VSL) of the Catholic University of America (CUA) and Energy*Solutions*, directed at improving waste loadings in borosilicate glasses, achieved maximum Na_2O and SO_3 loadings of about 24 wt% and 1.5 wt%, respectively, with an average Na_2O loading of 20.6 wt% across all of the Hanford LAW [4-8].

It has been proposed that phosphate glass systems have the potential to achieve higher waste loading in the LAW glass thereby improving processing economy while still producing a product that meets all of the WTP product quality requirements. Phosphate-based LAW glasses may well have the potential of offering higher waste loadings for components such as sulfur but it is much less clear that they have any significant loading advantage for sodium. In addition, phosphate glasses are an immature technology relative to borosilicate glasses for the vitrification of Hanford LAW. In general, early research on phosphate-based glasses has shown unacceptably high rates of corrosion of metallic melter components as well as crystallization on slow cooling leading to low-durability waste forms. However, more recent studies have shown promise in the ability to formulate iron phosphate (FeP) LAW glasses that may not demonstrate the drawbacks previously found in early phosphate formulations [9-11].

Recently, DOE initiated a program to assess the viability of using FeP glasses for LAW processing at Hanford [12]. This task was executed jointly between Missouri University of Science and Technology (MS&T), Savannah River National Laboratory (SRNL), Pacific Northwest National Laboratory (PNNL), Idaho National Laboratory (INL), Columbia Energy and Environmental Services (CEES), and VSL. The glass formulations were developed by MS&T. Processing of the glass formulation in a joule heated ceramic melter (JHCM) was assessed at PNNL while processing in a cold crucible induction melter was assessed at INL. VSL/Energy*Solutions* workscope for this task included corrosion testing of Inconel alloys and measurement of high temperature properties of the iron phosphate glass.

1.1   Test Objectives

The objectives of the work reported herein were to assess the corrosion of Inconel 690 and 693 in the FeP glass developed by MS&T and to measure key high temperature properties of the LAW iron phosphate glass.

Specific objectives of these tests were the following:

- Determination of the extent of corrosion of Inconel 690 and 693 in LAW FeP glass at 1050, 1100, and 1150°C
- Determination of the extent of corrosion of Inconel 690 and 693 in LAW FeP glass in the presence of an electric field
- Measurement of the high temperature specific heat of the LAW FeP glass
- Measurement of the high temperature density of the LAW FeP glass
- Measurement of the high temperature thermal diffusivity of the LAW FeP glass
- Calculation of the high temperature thermal conductivity of the LAW FeP glass from the above three measured properties.

The scope of this work was outlined in a Task Plan for the DOE EM-31 Technology Development & Deployment (TDD) Program Task 5.1.1 [13].

1.2   Test Overview

The FeP glass used in the tests was developed and prepared by MS&T based on the composition of LAW from Hanford tank AZ-101. The recommended melter feed processing temperature for this glass was 1050°C. This study examined two possible choices for an electrode material in a JHCM for the FeP glass. Inconel 690 is the alloy most widely used for electrodes and for other components in contact with glass in waste glass melters for borosilicate glass. A previous study by MS&T [14] compared the corrosion resistance of Inconel 690 and 693 in an earlier iron phosphate glass formulation and found that the corrosion rate of Inconel 690 was about twice that of 693 in a simple immersion test at 1050°C in alumina crucibles with renewal of the melt glass every 7 days for a total 155 days. In this work, Inconel 690 and 693 were tested for corrosion resistance to FeP under static glass contact conditions for 7 days at

1050, 1100, and 1150°C and for 14 days at 1050°C with renewal of melt glass at 7 days. The better-performing alloy (Inconel 693) was tested for 3 days at 1050°C with an applied electric field producing a surface current density of 10 A/in^2. In addition to dimensional material loss measurements, the tested coupons were also subjected to examination by scanning electron microscopy (SEM) with analysis by energy dispersive X-ray spectroscopy (EDS) to more completely evaluate the extent of corrosion. Dimensional measurements alone do not reveal the extent of compositional and microstructural alteration, which may indicate a much shorter service life than that suggested by simple material loss measurements.

High temperature specific heat, density, and thermal diffusivity were measured using the FeP glass supplied by MS&T. Those data were used to calculate the thermal conductivity of the FeP glass.

1.3   Quality Assurance

This work was conducted under a quality assurance program that is based on Nuclear Quality Assurance (NQA)-1 (2004) and NQA-2a (1990) Part 2.7 that is in place at the VSL. The program is compliant with applicable criteria of 10 CFR 830.120; Office of Civilian Waste Management DOE/RW-0333P, Quality Assurance Requirements and Description (QARD) Revision 20; the American Society of Mechanical Engineers (ASME) NQA-1, 2000 and 2004; and DOE Order 414.1 C, Quality Assurance. This program is supplemented by a Quality Assurance Project Plan for Washington River Protection *Solutions* (WRPS) work [15] that is conducted at VSL. Test and procedure requirements by which the testing activities are planned and controlled are also defined in this plan. The program is supported by VSL standard operating procedures that were used for this work [16]. QARD was not applicable because this is LAW work.

SECTION 2.0
EXPERIMENTAL METHODS

2.1   Introduction

The objectives of this work included a comparative evaluation of the corrosion resistance of two Inconel alloys, 690 and 693, in FeP glass under static conditions and with the application of an electric field, and measurement of the high temperature properties of the FeP glass. The FeP formulation used in these tests was prepared by MS&T and supplied to VSL where it was analyzed by XRF to verify composition prior to use (Table 2.1). The extent of glass-contact corrosion of Inconel 690 and 693 was evaluated at temperatures of 1050°C, 1100°C, and 1150°C for 7 days, and at 1050°C for 14 days with replacement of the FeP glass at 7 days. The test coupons were then sectioned and analyzed for their dimensional loss and internal structural damage to determine the effects of test temperature and time. In addition, the metal corrosion of Inconel 693 under an imposed electric field that produced an average current density of 10 A/in^2 at the coupon surface was assessed at 1050°C for 3 days.

Generally, Inconel alloys react with molten glass rather slowly at typical melter operating temperatures, which one of the reasons for their selection for use in waste glass melters. However, this presents challenges in assessing the corrosion damage to the alloy by a molten glass, particularly if it is judged solely from the dimensional loss determined in a short-term laboratory test. The interior structural damage incurred in the corrosion process, which can be assessed by electron microscopy, provides valuable additional information and is often more indicative of the extent and nature of the corrosion process. Key parameters for assessing the corrosion damage to Ni-Cr based super alloys such as Inconel 690 and 693 are:

- The dimensional loss of the test coupons
- Internal structural degradation, as reflected by grain boundary damage, oxidation, or glass melt intrusion
- Internal compositional alteration, as reflected by de-alloying or sensitization and, in particular, in the depletion of chromium, which, in general, is a critical element in Inconel alloys
- Oxide scale formation and characteristics

Table 2.2 summarizes the corrosion tests performed in this work and lists the test conditions and corresponding results. Table 2.2 also lists the ID codes for the test coupons and for the glasses remaining at the completion of the tests.

Measurements of high temperature specific heat, density, and thermal diffusivity of the FeP glass were performed in the temperature range of about 800 to 1150°C.

2.2 Sample Preparation for Corrosion Tests

2.2.1 Coupon Preparation for Standard Metal Corrosion Tests

Rectangular coupons of Inconel 690 and 693 were machined from the bulk material and their surfaces were polished (Figure 2.1). The coupons were 0.300 inch by 0.150 inch in cross-section and of sufficient length to be immersed in the molten glass to a depth of 0.9 inch. All dimensions of the coupons were measured by micrometer to better than 0.5 mil before the tests. The precision in the preparation of the parallel surface was better than 0.001 inch.

2.2.2 Coupon Preparation for Electrical Metal Corrosion Tests

These tests employed a concentric-cylinder geometry. The test coupon, which forms the center electrode for these tests, was machined from bulk Inconel 693 into a round pin with a diameter of 0.195 mm and a length of 22 mm. Inconel wire was welded to one end of the pin for electrical connection. The pin with attached wire was then inserted into an alumina protective sleeve and made to protrude from the sleeve by 10 mm.

2.2.3 Glass for Corrosion Tests

The FeP formulation used in these tests was prepared by MS&T and supplied to VSL.

2.3 Metal Glass-Contact Corrosion Tests

2.3.1 Standard Metal Glass-Contact Corrosion Test

Corrosion tests with molten glass were conducted using the experimental arrangement shown schematically in Figure 2.2. The experimental setup consisted of a 50 ml platinum crucible placed into a quartz holder. On the top of the crucible there is a cover with a 5 mm slot. The coupon is placed through the slot and suspended by a rod that is placed through a hole drilled through one end of the coupon. For each corrosion test, 70 grams of glass is melted at 1150°C (nominal) for 30 minutes; this quantity gives an ratio of the coupon surface area to the volume of glass (S/V) for these tests of 0.15 cm^{-1} and the crucible is filled to ¾ of its height (29 mm) with glass. The coupon with the lid is preheated to 800°C, allowing an oxide layer to form on the coupon, which is then placed into the crucible with the molten glass. The experimental setup is then placed into a furnace that is preheated to the desired test temperature (1050°C, 1100°C, or 1150°C). After the designated period of time, the setup is removed from the furnace, the coupon is extracted from the glass, and the glass melt is poured into a graphite mold for further analyses. The coupon with the glass coating is allowed to cool and then embedded in epoxy. For the extended tests, the coupon and lid are removed from the initial crucible after 7 days, excess glass is allowed to drip off the coupon, and the coupon with lid are placed in a crucible containing fresh glass. The glass from the first crucible is poured into a graphite mold

and sampled for further analysis. After the second 7-day period, the coupon and glass are removed according to the same procedure for further analysis.

The first 7-day test for both alloys was run at 1050°C, and the second at 1150°C. The Inconel 690 coupon failed dramatically during the 1150°C test, splitting at the glass-air interface area with the result that the lower portion of the coupon settled to the bottom of the platinum crucible and destroyed the crucible. As a result, the remaining standard corrosion tests for Inconel 690 were performed in alumina crucibles, as is standard practice in tests performed at MS&T [14]. However, the substitution of alumina crucibles resulted in a significant increase in the concentration of alumina in the FeP glass during the course of the test.

2.3.2   Electrical Metal Glass-Contact Corrosion Test

Corrosion tests in the presence of an electric field were conducted in molten glass at 1050°C. The test employs concentric cylinder geometry. The outer cylinder is normally fabricated from Inconel 690 and forms both the container for the molten glass and one of the electrodes. The inner cylinder, which is of much smaller diameter, is fabricated from the test material and forms the second electrode. In this way, a high current density is achieved at the test coupon while maintaining a low current density at the container and a relatively low total current, which avoids excessive joule heating. The entire assembly is installed in a vertical tube furnace set at the desired test temperature. The center electrode with attached wire is introduced inside the tube furnace after being inserted into an alumina protective sleeve and made to protrude from the sleeve by 10 mm. In the normal VSL procedure for this test, another Inconel wire is welded to the top edge of the Inconel 690 crucible for electrical connection. However, for the present electrical corrosion test with the FeP glass, due to excessive foaming in experiments using Inconel 690 crucible, a Pt/Rh crucible with a Pt/Rh wire was used. During the test, the center electrode is positioned at the center of the crucible and introduced into the glass melt to a depth of 12 mm, which allowed the alumina sleeve surrounding the center electrode to extend 2 mm into the melt. This 2-mm immersion helps to prevent enhanced corrosion of the center electrode at the air-glass melt line during the test (Figure 2.3).

In the present work it was found that the FeP glass tends to foam when heated in an Inconel 690 crucible, which compromised the test. As a result, after three unsuccessful attempts involving various heating schedules, a platinum/rhodium crucible was substituted for the Inconel 690 container for the electrical corrosion test. This foaming does not appear to be a result of reboil because it was observed only in Inconel crucibles, and not in platinum or alumina crucibles. Since the work scope was limited to corrosion testing and property measurements, additional studies were not done to identify the cause of this foaming.

The electric circuit for the tests is shown in Figure 2.4. A 60 Hz AC source was used to maintain a current density of 10 A/inch^2 at the center electrode pin. Over the entire duration of the electrical corrosion experiments (three days at 1050°C under ambient conditions), the actual current passing through the corrosion cell was controlled by monitoring the voltage across a precision resistor that was in series with the corrosion cell. The actual current passing through

the circuit to achieve the targeted 10 A/inch^2 current density was 1.0 A.

After the test coupon was removed from the corrosion setup, it was sectioned at 1 mm, 5 mm, and 9 mm from the bottom tip and the cross-sections were prepared for subsequent microscopic analysis.

2.4   Optical Microscopy

After each corrosion test, the reacted coupons were embedded in resin and then sectioned at the mid-point and polished. Both halves of the sectioned coupons were examined for corrosion characteristics (e.g., morphology of new, modified, and original phases, the texture of the reacted alloys, etc.) using a microscope. The thickness of the reacted coupon was measured using a measuring microscope, which has a precision of better than 0.05 mil (1.27 μm). Typically, 10 transverse lines were measured perpendicular to the length of the coupon. The overall uncertainty associated with these measurements is about 0.5 mil. The dimensional loss is calculated as half of the difference of the measured widths between the original and reacted coupons near the glass line (or sometimes referred as the *neck* if such a feature develops) and at the location corresponding to half of the immersed length of the coupon (referred to as the *half-down* position). The measurements are illustrated in Figure 2.5. The sectioned coupons were further characterized using Scanning Electron Microscopy - Energy Dispersive X-ray Spectroscopy (SEM-EDS).

2.5   Scanning Electron Microscopy - Energy Dispersive X-ray Spectroscopy (SEM-EDS)

Scanning electron microscopy was performed using a JEOL JSM-5910LV SEM equipped with an Oxford INCA 300 digital imaging and EDS system to characterize the microstructure and compositional alterations of alloy materials after corrosion testing. Magnifications used typically ranged from 25× to 5,000×. EDS was used to analyze the chemical composition of the glass, crystalline oxide phases, and the corroded materials. SEM measurements supplement information on the structurally damaged zone provided by optical microscopy. Elemental profiles were obtained using EDS analysis either in line-scanning or selected point acquisition mode from the glass-metal interface to the center of the coupon.

2.6   Compositional Analysis

Glass samples were taken and analyzed before and after the corrosion experiments. This information provides an indicator of the corrosion progress that is complementary to the coupon analyses.

The primary method used for glass analysis was X-ray fluorescence (XRF) on powdered glass samples. A Thermo Scientific ARL 9400 wavelength dispersive XRF spectrometer with extended light-element capability was used for this purpose. Lithium and boron cannot be determined by XRF, but since these elements are not significant components of the FeP glass,

the digestion and solution analysis procedure normally used to determine them was not necessary.

2.7   Specific Heat

The specific heat of glass melts and solid glass samples was measured by Differential Scanning Calorimetry (DSC). Under a controlled environment and constant heating rate, the heat flux between the reference and the sample were continuously measured by two highly sensitive thermocouples. After proper baseline correction, the specific heat as a function of temperature can be calculated from the observed heat flux.

A Setaram^{TM} MHTC96 with TG-DSC module was used for measurement of specific heat of glass and glass melt samples. The system was calibrated using National Institute of Standards and Technology (NIST)-traceable standards under identical conditions as used for the samples and over the same temperature range for the measurement of specific heat of melt and glass samples. All measurements of the blank, NIST standard, and glass samples, were made at a heating (or cooling) rate of 5°C/minute in an ambient environment controlled by regulated air flow through the sample chamber. For each measurement, about 500 mg of sample was loaded into a Pt sample cup and melted in a box furnace at 1150°C before the DSC measurements. Data from three consecutive heating and cooling cycles were collected, calculated, and averaged for the final presented data; any obvious outlying points in the raw data were removed prior to averaging. The low temperature end (above 300°C) was limited by the temperature control of the calorimeter and the high temperature end was set to be below 1050°C to minimize corrosion problems of the Pt-ware in the DSC module.

2.8   Density

Archimedes' method was used for determination of glass melt density at controlled temperatures [17]. In a typical experiment, a bob of known mass and dimension is weighed separately in air and in a glass melt of interest. The ratio of the buoyancy, which accounts for the weight difference measured in air and in the melt, to the volume of the bob is equal to the density of the glass melt.

A calibrated analytical balance configured for bottom-hook application was located above a high temperature vertical tube furnace, with adequate thermal insulation in place to protect the balance. A Pt-10%Rh bob of known volume and mass was suspended from the bottom hook of the balance by a 20 mil diameter Pt-10%Rh wire and immersed in the glass melt. The temperature of the sample was determined by a calibrated thermocouple. The density calculation was calibrated periodically by measuring the density of molten reagent grade NaCl [18, 19].

About 100 grams of the glass melt was contained in a Pt-10%Rh cylindrical crucible placed in the hot zone of the tube furnace. For buoyancy measurement, the bob was fully immersed in the glass melt while being suspended from the analytical balance. A second bob of

different volume and mass was also used in the measurement. The difference of the observed buoyancy and volume of the two bobs at a given temperature was used in the calculation of the density of the FeP melt in order to eliminate the effect of surface tension. The experimental temperature range over which the density was measured was largely determined by the condition of the glass melt. For the FeP glass studied in the present work, the low temperature end was limited to 800°C by the viscosity and the tendency for crystallization of the glass sample.

2.9   Thermal Diffusivity

A modified Ångström method was used for measurement of the thermal diffusivity of glass melts at high temperature. The method can be applied to a material in cylindrical geometry, the surface of which is subjected to periodic temperature variations around a given mean temperature, at a given amplitude and period, created by a concentrically aligned cylindrical heat source. The propagation of heat waves is monitored radially at two locations. The thermal diffusivity of the substance at the given mean temperature can be calculated from the observed phase lags of the temperature waves.

The test glass was loaded into a long, cylindrical crucible which was placed in the center of the heat source. Two S-type thermocouples were used to measure temperature, with one at the center and the other near the inner surface of the cylinder. The sinusoidal temperature changes of the furnace and the temperatures measured by the two monitoring thermocouples were recorded via an A/D converter and stored digitally on a PC for subsequent data analysis. The method of calculation of thermal diffusivity from the experimentally measured temperature wave at two locations is described in detail in the associated VSL procedure.

Cylindrical crucibles ~8 inch tall and 3.1 inch internal diameter were fabricated from seamless Inconel 601 tube. When the crucible was fully loaded with glass, the ratio of the immersion depth (~3 inch) of the thermocouples to the distance between the two thermocouples (~1 inch) was almost 3, a value considered sufficient to be able to ignore fringe effects [20]. For each of the average temperatures, the heat wave was modulated by ±15°C with a period of 120 minutes. The obtained sinusoidal waves from each of the two monitoring thermocouples were then analyzed to determine the phase lag between the two locations separated by a known distance. The thermal diffusivity at the test temperature was calculated on the basis of the phase lag and the distance following the method derived by Van Zee and Babcock [21].

SECTION 3.0
RESULTS OF CORROSION TESTS

3.1   Standard Glass Contact Metal Corrosion

Standard glass contact metal corrosion tests were performed for all Inconel 690 and 693 coupons at 1050°C, 1100°C, and 1150°C for seven day durations, and for Inconel 693 at 1050°C for an extended 14 day period. Coupon alteration results are summarized in Table 3.1, which also provides ID codes for the various coupons and for the test glasses. Table 3.2 provides the results of XRF analysis on the various glasses at the completion of the respective tests. Glasses FeP1050-3, FeP1050-5, and FeP1100-1 are from the Inconel 690 tests that were run in alumina crucibles, and are much higher in alumina and much lower in chromium than the starting glass. It is evident that the dissolution of alumina from the crucible significantly alters the composition of the glass and may well affect the chemistry of the glass-coupon interaction. In addition, dissolution of alumina into the melt is likely to increase the viscosity of the glass melt, and reduce the rate of corrosion of Inconel in the phosphate glass melt.

Normalized values are reported for the glass composition analysis by XRF. The XRF analyzed Cr_2O_3 concentration in the MS&T phosphate glass before testing is higher than target (3.26 wt% vs 2.70 wt%). Analysis of another 3 batches of phosphate glass from MS&T gave an average Cr_2O_3 concentration of 3.16 wt%. After corrosion tests, the samples tested in platinum crucibles showed Cr_2O_3 concentrations in the range of 2.14 to 2.82 wt%, with most values less than the target of 2.70 wt%. This is probably due to the formation and settling of Cr-containing crystals that depleted Cr in the bulk glass. Cr_2O_3 concentration in glasses tested in alumina crucibles varied from 0.3 to 1.07 wt% versus a target of 2.70 wt%. Part of the reduction in Cr_2O_3 concentration is due to the dilution of the glass from dissolution of alumina from the crucible. The probable major reason is the formation and settling of Cr-containing crystals that depletes Cr from the bulk glass.

3.1.1   Standard Metal Glass-Contact Corrosion Test: 7 Days at 1050°C

Figure 3.1 displays three micrographs of Inconel 690 coupon INC690-FeP1050, corrosion tested for 7 days at 1050°C. Grain boundary attack is evident in the micrographs to a maximum depth of about 70 μm. Figure 3.1a shows the surface of the coupon near the half-down region to a depth of about 500 μm with attack along grain boundaries evident to a depth of up to 70 μm. Figure 3.1b shows the metal near the surface in greater detail with some inclusions identified. The Al_2O_3 and Cr_2O_3 are corrosion products, while the MgO is probably due to a minor impurity in the original Inconel. Figure 3.1c shows the metal surface and the detached surface scale with adhering glass, and identifies the significant phases present: Cr_2O_3, Al_2O_3, and Fe-Cr spinel (chromite, $FeCr_2O_3$). Figure 3.2 shows a concentration profile based on the EDS line scan for Cr with depletion evident to a depth of about 100 μm. The Cr concentration near the

surface is about 22 wt%, representing a relative loss of about 27% compared to the original Inconel.

Figure 3.3 displays three micrographs of Inconel 693 coupon INC693-FeP1050 and its detached scale. Grain boundary attack is evident in the micrographs to a maximum depth of about 200 µm. Figure 3.3a shows the surface of the coupon near the half-down region to a depth of about 500 µm with attack along grain boundaries evident to a depth of up to 200 µm. Figure 3.3b shows the metal near the surface in greater detail with some inclusions identified. Again, Al_2O_3 is evident and there are some Zr-containing regions. Figure 3.3c shows the detached scale with adhering glass. The left surface was originally in contact with the metal. The outer surface of the scale appears to be mostly Cr_2O_3 with some Fe and Al. There are some bright regions near the metal contact side of the scale which have a complex composition (Ni, Fe, Cr, P, Al, O). It is not clear whether the phosphorus is present as phosphate or phosphide, nor is it clear whether the Ni, Fe, and Cr are reduced or oxidized. Figure 3.4 shows a concentration profile based on the EDS line scan for Cr with depletion evident to a depth of about 100 µm. The Cr concentration near the surface is about 27.5 wt%, representing a relative loss of about 8.4% compared to the original Inconel. Although the grain boundary attack is deeper in the Inconel 693 than in the 690, and the width of the Cr depletion region is about the same, the magnitude of the Cr depletion is significantly lower in 693. The line scan included a full X-ray spectrum at every point so that all detectable elements could be checked and mapped. The major difference between Inconel 690 and Inconel 693 is that the latter contains about 3 wt% aluminum to improve resistance to certain types of corrosion. Inspection of the line scan for Al revealed that it begins a steady decline at about 300 µm from the surface and was down to 0.3 wt% at 100 µm from the surface, and to less than 0.1 wt% at the surface itself. This Al loss might indicate that Inconel 693 could lose its apparent superiority over 690 relatively quickly, and then be subject to a much higher rate of attack.

3.1.2 Standard Metal Glass-Contact Corrosion Test: 7 Days at 1100°C

Figure 3.5 displays micrographs taken of Inconel 690 coupon INC690-FeP1100 and its detached scale. Grain boundary attack is evident in the micrographs to a maximum depth of about 175 µm. Figure 3.5a and 3.5b highlight the damaged region in the Inconel 690 near the half-down region of the coupon and identify typical phases that are observed. In Figure 3.5b, there are two regions where Al_2O_3 is present with some silica, and in one case with Zr. Although silica is present in FeP glass only at about 5.4 wt%, it is frequently found in subsurface phases in the corroded coupons. Figure 3.5c shows a cross section of the detached scale and identifies some typical phases present. Figure 3.6 shows a concentration profile based on the EDS line scan for Cr with depletion evident to a depth of about 250 µm. The Cr concentration near the surface is about 18 wt%, representing a relative loss of about 40% compared to the original Inconel 690.

Figure 3.7 displays micrographs taken of Inconel 693 coupon INC693-FeP1100 and its detached scale. Grain boundary attack is evident in the micrographs to a maximum depth of about 350 µm. Figure 3.7a shows the extent of grain boundary and surface attack. Figures 3.7b and 3.7c detail the grain boundary attack and the phases present, which are primarily alumina

and silica. Figure 3.7d shows the detached scale and adherent glass. The corrosion products in the outer scale and glass appear to be a spinel containing Al, Cr and Fe, while those closer to the interface include small granules of Inconel metal residue containing phosphorus in an apparent reduced state. Figure 3.8 shows a concentration profile based on the EDS line scan for Cr with primary depletion evident to a depth of about 200 μm, the value reported in Table 3.1, with a smaller depletion possibly present to a depth of about 400 μm. The Cr concentration near the surface is about 24 wt%, representing a relative loss of about 20% compared to the original Inconel 693. Again, although the grain boundary attack is deeper in the Inconel 693 than in the 690 and the width of the major Cr depletion region is about the same, the magnitude of the Cr depletion is significantly lower in 693. Here again, independent examination of the Al X-ray line scan in the INC693-FeP1100 coupon revealed a steady decline in Al_2O_3 concentration over the entire width of the line scan from about 2.5 wt% at a depth of about 500 μm, which is already below the concentration in the starting metal, to about 0.1 wt% at the coupon-glass interface.

3.1.3   Standard Metal Glass-Contact Corrosion Test: 7 Days at 1150°C

The Inconel 690 coupon failed during testing for 7 days at 1150°C. The coupon split at the neck area and the lower portion settled to the bottom of the platinum crucible in which the test was being run, reacting with and destroying the crucible, resulting in the loss of the FeP glass. Figure 3.9 displays several photographs and SEM micrographs of the remaining upper segment of the INC690-FeP1150 coupon. Figure 3.9a is a photograph of the remaining upper portion of the coupon still attached to the Zirmul support and crucible cover that was used during the test. Figure 3.9b shows the damaged coupon after it had been removed from the cover, and Figure 3.9c shows the coupon after it had been mounted in epoxy and cross sectioned through the tip of the failure zone. The same type of catastrophic failure, accompanied by extensive vapor phase attack, was observed previously in tests on an earlier FeP glass formulation conducted at 1130°C [22].

The SEM micrographs and EDS work on the remaining upper portion of the INC690-FeP1150 coupon yield some interesting data, which must be interpreted cautiously because of the uncertain conditions prevailing after the failure of the coupon. Figure 3.9d is a low magnification backscatter SEM micrograph of the sectioned tip area of the remaining upper portion of the metal coupon and its adherent scale. The Cr content of the tip area of the remaining upper portion was severely depleted to around 10 wt%, about a 67% relative depletion from the original Inconel 690, to a depth of at least 800 μm from the surface. The scale on the tip contains an assortment of spinels and other oxides, some chromium (and other) phosphates, and near the metal-scale interface, mixed phosphides of Cr, Ni, Fe, Mn, and Ti. At the surface and within the remaining metal there is severe attack by sulfidation and phosphidation with the sulfide being primarily chromium and the phosphide a mixture of Cr, Fe, and Ni, but rich in nickel. There are also numerous small (0.1 to 2 μm) pockets of bismuth in the coupon near its surface and to a depth of about 1 mm along cracks infiltrating the coupon. Figures 3.9e and 3.9f show details of the corrosion at the metal-scale interface. At the center of the coupon, in addition to the phosphides and sulfides, there is crystallization along the original grain boundaries of what appears to be nearly pure chromium. These Cr crystals are also seen within the grains, normally with platelet morphology. The platelets are oriented with their narrow axis along three specific

orientations at 60° angles to each other. Within some of the larger Cr crystals, there are regions or crystals of a Ti-Cr intermetallic with an atomic ratio Ti:Cr of about 6:1.

The corrosion processes for FeP glass in contact with Inconel 690 at 1150°C are clearly very aggressive and complex. Although the nominal melter operating temperature for this FeP glass formulation is 1050°C (i.e., 100°C lower than the temperature at which this test was performed), in view of the extent of the damage, that is unlikely to provide an adequate safety margin for typical nuclear waste glass melter designs. As noted above, because corrosion severed the coupon at the neck area allowing the lower portion of the coupon to settle into contact with and react with the platinum crucible in which the test was being conducted, the detailed corrosion features observed in the SEM micrographs may not be entirely representative of what would have happened if the test was run in a crucible made of a different material. Nevertheless, the very failure of the coupon indicates that Inconel 690 is probably not a good choice for long term use in phosphate glass melters.

Figure 3.10 displays SEM micrographs of Inconel 693 coupon INC693-FeP1150 and its detached scale. Grain boundary attack is evident in the micrographs to a maximum depth of about 40 μm. This is considerably smaller than the 350 μm depth observed in coupon INC693-FeP1100, but it should be noted that the material loss from this coupon was considerably greater than for INC693-FeP1100, and the loss may have been in the area of greatest grain boundary damage. Furthermore, inspection of Figure 3.10a shows a rather dense subsurface layer of nodules, which are identified in Figures 3.10b and 3.10c as Al_2O_3, and which may be sealing the grain boundaries retarding further attack. Figure 3.10c indicates that the scale on the coupon is primarily Cr_2O_3, which is intergrown with a small amount of an Fe-Cr-Al spinel. Figure 3.11 shows a concentration profile based on the EDS line scan for Cr. The slope of the depletion curve is very small, but it appears the depletion is evident to a depth of about 300 μm. The Cr concentration near the surface is about 27 wt%, representing a relative loss of about 10% compared to the original Inconel. Independent examination of the Al X-ray line scan in the INC693-FeP1150 coupon revealed Al depletion to a depth of about 300 μm, about the same depth as seen in the 1050°C test with Inconel 693, and not as deep as the depletion in the INC693-FeP1100 coupon. Recall, however that the material loss from this coupon is greater than in either of the two lower temperature tests, so the depth of depletion appears smaller than it would have without the greater material loss.

3.1.4   Standard Metal Glass-Contact Corrosion Test: 14 Days at 1050°C

Micrographs of Inconel 690 coupon INC690-FeP1050-2 and of the detached scale originally adhering to the coupon are displayed in Figure 3.12. A partially delaminated layer ranging from 15 to 20 μm wide is visible on the coupon in Figures 3.12a and 3.12b, which are SEM micrographs taken in the half-down region of the coupon. It is not clear what may have caused this layer to form and partially spall off. The attacked grain boundary regions extend to a depth of about 100 μm below the surface and all show the presence of Al_2O_3. The aluminum probably comes from the Inconel 690 since, although it is not normally reported on alloy spec sheets for Inconel 690, it is usually present, although at much lower levels than in 693. The

corrosion products evident in the coupon scale shown in Figure 3.12c are a Cr-Fe-Al spinel, Cr_2O_3 containing small amounts of Fe and Al, and a trace of Si. Figure 3.12d shows that fragments of the Inconel 690 are present in the scale that detached from the coupon when it was taken off. Figure 3.13 shows a concentration profile based on the EDS line scan for Cr with depletion evident to a depth of about 250 μm. The Cr concentration near the surface is about 21 wt%, representing a relative loss of about 30% compared to the original Inconel 690.

The Inconel 693 coupon INC693-FeP1050-2 is shown in Figure 3.14. Figure 3.14a is an SEM micrograph of the coupon and its contact surface with the FeP glass taken near the half-down region and showing a severely reacted band 20 to 50 μm wide along the surface populated with nodular Al_2O_3. The grain boundary attack runs to a depth of about 200 μm. Figure 3.14b details the grain boundary attack showing the presence of Al_2O_3. Figure 3.14c shows a portion of the detached scale with the commonly observed Fe-Cr-Al spinel present in it. The Mg-Al area in the grain boundary region has the correct atomic proportions for the classic spinel $MgAl_2O_4$. The Mg was probably an impurity in the original Inconel rather than something taken up from the test glass. Figure 3.15 shows a concentration profile based on the EDS line scan for Cr with depletion evident to a depth of about 325 μm. The Cr concentration near the surface is about 27.6 wt%, representing a relative loss of about 8% compared to the original Inconel 693. Inspection of the line scan for Al revealed that it began a steady decline at about 350 μm from the surface and was down to 0.3 wt% at 40 μm from the surface, and to about 0.1 wt% at the surface itself.

3.2   Electrical Metal Glass-Contact Corrosion

Since Inconel 693 clearly performed better than 690 on the standard corrosion tests, it was further evaluated in a 3-day electrical corrosion test at 1050°C with a current density of 10 A/in^2. At the completion of the test, the coupon was removed, mounted in epoxy and sectioned at 1.5, 3, and 9 mm from the lower tip of the coupon. These sections were then remounted in a second standard SEM epoxy mount and polished for visible light optical microscopy and SEM observation and measurements. From the outset it should be noted that the microstructure of the cross sections at different distances from the tip look rather similar except at the perimeter. Also worthy of note is the fact that the degree of damage within the coupon is much more severe in the 3-day test with current flow than it is in the longer duration static corrosion tests at the same temperature. Examination of the images also suggests that not all of the damage and secondary phase growth originated at grain boundaries.

3.2.1   Electrical Metal Glass-Contact Corrosion: 1.5 mm from Tip

SEM images of the 1.5 mm section in Figure 3.16 reveal a greater degree of edge damage than the sections at 5 mm and 9 mm. The focusing of current flow at the coupon tip probably accounts for the difference in edge damage. Referring back to Table 3.1, no cross section loss was noted at 1.5 mm, which is appears surprising at first because examination of Figure 3.16a gives the impression that a significant amount of the perimeter has spalled off, as evidenced by

some segments remaining on the coupon. However, it also appears that the secondary phases forming within the coupon probably caused expansion of the remaining material, resulting in the final measured diameter being the same as the original.

There are a variety of phases that formed in the coupon during the current flow test. Figure 3.16b is a more detailed micrograph of part of the cross section where the X-ray line scan to determine element distribution profiles was done. The dark, round, somewhat fuzzy spots in the central region of this 1.5 mm section are not corrosion features, but carbon contamination. Figure 3.16c shows the edge region of the coupon in greater detail with three commonly occurring phases identified based on qualitative composition. A fourth phase containing only Cr and N was also observed less frequently than the other three. The presence of reduced phases (nitrides and phosphide) is a clear difference between the electrical corrosion tests and the static tests. The Cr-Ni phosphide phase is found here only in a band between 50 and 100 μm beneath the coupon surface. The amount of phosphorus present in the latter phase is small, only 2 to 4 atom%, but it is significant that some phosphorus is entering the coupon and that it is found in a distinct phase. The absence of the Al_2O_3 phase in the grain boundaries is also a significant difference between the static and electrical corrosion tests.

The scale on the coupon did not polish well in the prepared SEM mount of this section, so it is not well represented in the micrograph. However, careful examination of the micrograph in Figure 3.16a revealed that it ranged from 20 to 60 μm in thickness and contained primarily Cr_2O_3 with a little Fe, and a Cr-Fe-Al spinel with a composition close to chromite ($FeCr_2O_4$). In general, the scale on the electrical corrosion pin was less dense and varied more in thickness from place to place than that observed on the static test coupons.

Figure 3.17 shows a concentration profile based on the EDS line scan for Cr, with depletion evident to a depth of about 200 μm. The Cr concentration near the surface is about 21 wt%, representing a relative loss of about 30% compared to the original Inconel 693. Inspection of the X-ray line scan for Al revealed that it begins a sharp decline at about 370 μm from the surface to about 230 μm from the surface, where it is down to 0.1 wt%, and to less than 0.1 wt% at the surface itself. Much of this Al depletion is due to the concentration of Al in the nitride phase.

3.2.2   Electrical Metal Glass-Contact Corrosion: 5.0 mm from Tip

Figure 3.18a shows the entire cross section of INC693EC-1150-B, which is the section cut 5.0 mm from the pin tip. There is some surface roughness on the coupon perimeter, attributable to moderate swelling and cracking of the coupon, but much less than in the case of the 1.5 mm section. The secondary phases within about 150 μm of the surface appear to have a slightly finer grain size than in the1.5 mm section. Figure 3.18b is a more detailed micrograph of part of the cross section where the X-ray line scan to determine element distribution profiles was done. Figure 3.18c shows the edge region of the 5.0 mm section and a portion of its scale in even greater detail with the principal phases identified. The same phases are observed in this section that were observed in the 1.5 mm section, but the Cr-Ni phosphide phase in the 5.0 mm section is

found in a narrower band about 125 μm beneath the pin surface. The scale on the surface of this section is highly variable in thickness, running from 0 to 100 μm, but it contains the same phases seen before: Cr_2O_3 containing a little Fe, and Cr-Fe-Al spinel with a composition close to chromite ($FeCr_2O_4$).

Figure 3.19 shows a concentration profile based on the EDS line scan for Cr with depletion evident to a depth of about 220 μm. The Cr concentration near the surface is about 17 wt%, representing a relative loss of about 43% compared to the original Inconel 693, and a greater loss than measured in the 1.5 mm section. The greater relative loss here may simply be because more of the original metal was retained in the 5.0 mm sample. The material lost from the 1.5 mm section may have had similar Cr depletion but was not available for measurement. The X-ray line scan for Al showed a similar behavior to the one described above for the 1.5 mm section of the pin.

3.2.3 Electrical Metal Glass-Contact Corrosion: 9.0 mm from Tip

Figure 3.20a shows the entire cross section of INC693EC-1150-C, which is the section cut 9.0 mm from the pin tip. The 9.0 mm section looks very similar to the 5.0 mm section, but it is the only one of the three sections that exhibited a measurable loss of diameter after the test. Figure 3.20b is a more detailed micrograph of part of the cross section where the X-ray line scan to determine element distribution profiles was done. Figure 3.20c shows the edge region in greater detail, and Figure 3.20d is a subsection of Figure 3.20c where spot analyses of typical phases are given. Note again that the high-Zr areas (arrows 3 and 6) are irregularities in the original Inconel 693 and not corrosion products. Figure 3.20e is an SEM micrograph of a detached section of coupon scale and adherent glass with three common phases identified.

Figure 3.21 shows a concentration profile based on the EDS line scan for Cr, with depletion evident to a depth of about 180 μm. The Cr concentration near the surface is about 20 wt%, representing a relative loss of about 33% compared to the original Inconel 693. Again, the X-ray line scan for Al in the 9.0 mm section showed a similar behavior to those in the other two sections. Here the line scan for Al began its steep decline at about 340 μm from the surface, dropping to about 0.5 wt% at 220 μm from the surface, and then declining more gradually to less than 0.1 wt% at the surface itself.

3.3 Summary of Corrosion Test Results

Metal corrosion tests were conducted at 1050, 1100, and 1150°C using an FeP LAW glass formulated for melt processing at 1050°C. Inconel 690 and Inconel 693 coupons were tested. Standard metal corrosion tests for 7 and 14 days at 1050 and 1100°C showed acceptable rates of corrosion for both Inconel 690 and Inconel 693. Corrosion characteristics such as coupon dimension loss, corrosion depth, and chromium depletion were comparable for Inconel 690 and Inconel 693 tested in the FeP LAW glass at 1050 and 1100°C, and Inconel 690 tested in a borosilicate LAW glass at 1130 and 1230°C [23]. The borosilicate LAW glass and the FeP LAW

glass were formulated for melt processing at 1150°C and 1050°C, respectively. The FeP LAW glass has a melt viscosity of about 40 to 60 poise in the temperature range of 1050 to 1100°C [24], which is similar to the viscosity of about 50 poise for the borosilicate LAW glass at 1150°C. However, Inconel 690 coupon corrosion tested in the FeP LAW glass at 1150°C showed severe damage, with the coupon failing at the neck region during the test. The Inconel 693 coupon, however, did not show excessive damage during the 1150°C test in the FeP LAW glass. In general, Inconel 693 performed better than Inconel 690 in the corrosion tests with FeP LAW glass, which was also observed in a previous corrosion study [14]. The better performance of Inconel 693 in corrosion tests with the FeP LAW glass is most likely due to the presence of Al_2O_3 in the Inconel 693 alloy that inhibits corrosion. Since part of the Inconel 690 coupon from the 1150°C test fell in the melt and damaged the platinum crucible, some of the later tests were conducted in alumina crucibles, as was the case in the earlier study [14]. As is evident from Table 3.2, use of alumina crucible significantly affects the composition of the FeP glass during the test and the results from the test should be used with caution. Tests in alumina crucibles are likely to underestimate the extent of corrosion due to dissolution of Al_2O_3 from the crucible, which changes the composition of the glass during the test.

Inconel 693 was also corrosion tested in the FeP LAW glass at 1050°C and 10A/inch^2 current density. The coupon after 3 days of testing in the presence of the electric field showed the formation of several secondary phases, including nitrides and phosphides. The reduced phases, such as nitrides and phosphides, were not observed in coupons that were corrosion tested in the FeP glass without an electric field. The formation of secondary phases probably caused expansion of the coupon, making assessment of material loss by measurement of coupon dimensions unreliable. Another important difference between the coupons from tests with and without the electric field is the behavior of Al_2O_3 present in Inconel 693. In corrosion tests on Inconel 693 without an electric field, Al_2O_3 is found in the grain boundaries, potentially inhibiting corrosion, whereas Al_2O_3 is not found in the grain boundaries of the coupons tested in the presence of an electric field.

In summary, reduction of the nominal processing temperature of the FeP glass to 1050°C is certainly advantageous with respect to materials corrosion. However, the catastrophic failure of Inconel 690 in tests at 1150°C, as also observed in a previous study [22] performed with an earlier FeP formulation, would allow little safety margin for that material. Inconel 693 appears to provide significantly better performance in the FeP glass than Inconel 690. However, additional work should be performed, particularly on the effects of electric current, to better understand the evolution over longer periods of time of the alteration phases and morphologies identified in the present work and their consequences for long-term, in-service performance.

SECTION 4.0
RESULTS OF PROPERTY MEASUREMENTS

4.1 Specific Heat Data

Figure 4.1 shows the specific heat of the LAW FeP glass as a function of temperature. The data are listed at ten-degree intervals in Table 4.1. Over the temperature range of 340°C to 540°C, the specific heat data were collected during heating, while over the temperature range of 730°C to 1010°C, the data were collected during cooling. In the intermediate temperature range from 550°C to 720°C, the specific heat values were interpolated because of excessive crystallization of the glass that prevented direct measurement of the specific heat in this temperature range. The reproducibility of the specific heat values is expected to be about ±15%.

The specific heat data for the FeP glass, from 340°C to slightly above the glass transition temperature, varies with temperature in a manner similar to those of two LAW borosilicate glasses previously developed for ORP [25]. The magnitudes of the specific heat values also are similar, expect that the peak specific heat values slightly above the glass transition temperatures were slightly higher (0.1 – 0.2 J/g·K higher) for the borosilicate glasses, as compared to the FeP glass. The two LAW borosilicate glasses have glass transition temperatures above 500°C (~520°C and 535°C), while the FeP glass showed a glass transition temperature about 100°C lower (~417°C). In the temperature range above the glass transition temperature, the variation in specific heat with temperature is different for the FeP glass as compared to the two LAW borosilicate glasses [25]. In particular, in that region, the specific heat values for the two LAW borosilicate glasses decrease with temperature, whereas they increase slightly for the FeP glass. The difference in behavior may be due to the heavy crystallization observed in the FeP glass at temperatures somewhat above the glass transition temperature.

4.2 Density Data

Figure 4.2 and Table 4.2 show the experimentally determined density data for the FeP glass. The density was measured at 800, 900, 1000, 1050, and 1075°C for the FeP glass melt. The lowest temperature was limited by crystallization of the glass melt. From Figure 4.2, the density of the FeP glass decreases almost linearly with temperature. The change in melt density over a range of 275°C is about 2.9 %. Compared to the other waste glasses shown in Figure 4.2, the FeP glass shows densities that are near the high end of the range. However, the change in density with temperature follows a trend that is similar to those of the other glasses. The LAW FeP glass shows density values that are higher than those for the LAW borosilicate glass LAWA44, though both are well below the WTP density limit of 3.7 g/cc at room temperature [26].

4.3   Thermal Diffusivity Data

Figure 4.3 and Table 4.3 show experimentally determined thermal diffusivity data for the FeP glass melt. The thermal diffusivity was determined at 800, 900, 1000, 1050, and 1075°C for the FeP glass melt. The low temperature end was limited by crystallization. Foaming was suspected in the glass melt during data collection at 1050 and 1075°C. The thermal diffusivity data for the FeP glass melt, along with data for four other waste glasses [25], are given in Figure 4.3. WTP-C106 and HLW-E-A127 are HLW borosilicate glasses and LAWA44 and ORPLA20 are LAW borosilicate glasses. The thermal diffusivities of all four of the borosilicate glass melts increase with temperature, especially above 1000°C, with LAWA44 showing the smallest increase. In contrast, the FeP glass melt does not show any increase in thermal diffusivity with temperature.

The thermal diffusivity is typically weakly temperature dependent if the temperature is not too high. At high temperatures (above 800-1000°C), in addition to conduction, radiation starts to contribute significantly to the energy transfer. Since the emissive power increases with the fourth power of the absolute temperature, a steeper positive slope ultimately develops at high temperatures, as was observed above 1000°C for the two HLW borosilicate glasses and to a lesser extent for the two LAW borosilicate glasses. The absence of any such effect in the FeP glass melt may be due to the onset of foaming above 1000°C, which may have decreased the otherwise rising contribution to thermal diffusivity from radiation.

4.4   Thermal Conductivity Results

The thermal conductivity (κ, J/s.cm.K) is defined in terms of the heat flux (the rate of heat transfer per unit area) through a material that is subjected to a temperature gradient. For a one dimensional situation, Fourier's law is expressed as:

$$\text{Heat Flux} = -\kappa \, (dT/dx) \tag{4-1}$$

where (dT/dx) is the temperature gradient. The thermal conductivity can be measured directly by experimental methods or calculated from other material properties using the equation:

$$\kappa = \alpha \, \rho \, C_p, \tag{4-2}$$

where α is the thermal diffusivity (cm^2/s), ρ is the density (g/cm^3), and C_p the specific heat at constant pressure (J/g.K). As reported above, data for thermal diffusivity, density, and specific heat have been collected for the FeP glass in the present work, as well as for four representative WTP waste glasses melts in previous work [25]. The thermal conductivity can then be calculated directly from the measured quantities using equation (4-2).

Table 4.4 lists the calculated thermal conductivity of the FeP glass melt at 800, 900, 1000, 1050, and 1075°C from the measured values of specific heat, density, and thermal diffusivity. It should be noted that the specific heat data at 1000°C were used for calculations at 1050 and 1075°C. The overall error of the calculated thermal conductivity was estimated from

the error of each of the three property measurements. Using conservative standard deviations of 0.1 J/g.K for specific heat, 0.01 g/cm^3 for density, and 0.001 cm^2/s for thermal diffusivity, the propagated error for thermal conductivity was previously estimated to be around 0.006 J/s.cm.K, or roughly 22% [25].

As defined in equation (4-1), the thermal conductivity describes the ability of a material to conduct heat under an imposed temperature gradient. Doubling the thermal conductivity implies that twice as much heat is conducted per unit area for a given time and temperature gradient. As shown in Table 4.4 and Figure 4.4, the thermal conductivity of the FeP glass melt varies little with temperature, in contrast to the other glass data presented in Figure 4.4. The FeP glass melt shows lower thermal conductivity than any of the borosilicate waste glasses. Overall, for these glass compositions and temperatures, the behavior of the thermal conductivity is determined largely by that of the thermal diffusivity. The lower thermal conductivity would likely translate into slower rates of cooling of filled glass containers (assuming the same geometry). This could have impacts on facility cycle times and the extent of crystallization during container cooling.

The crystallization observed at temperatures above about 550°C and foaming suspected during thermal diffusivity data collection at 1050 and 1075°C should be noted when using the data on the high temperature properties reported here for the FeP glass melt.

SECTION 5.0
SUMMARY AND CONCLUSIONS

Tests were conducted using an FeP glass developed by MS&T with the objective of assessing the viability of this glass formulation for LAW treatment at Hanford. Testing of the glass formulation for factors important in waste processing such as product quality and feed processing characteristics were conducted at MS&T, SRNL, PNNL and INL. The results of corrosion testing and high temperature property measurements are presented in this report.

Metal corrosion tests were conducted at 1050, 1100, and 1150°C using an FeP LAW glass formulated for melt processing at 1050°C. Inconel 690 and Inconel 693 coupons were tested. Standard metal corrosion tests for 7 and 14 days at 1050 and 1100°C showed acceptable rates of corrosion for both Inconel 690 and Inconel 693. Corrosion characteristics such as coupon dimension loss, corrosion depth, and chromium depletion were comparable for Inconel 690 and Inconel 693 tested in the FeP LAW glass at 1050 and 1100°C, and Inconel 690 tested in a borosilicate LAW glass at 1130 and 1230°C [23]. The borosilicate LAW glass and the FeP LAW glass were formulated for melt processing at 1150°C and 1050°C, respectively. The FeP LAW glass has a melt viscosity of about 40 to 60 poise in the temperature range of 1050 to 1100°C [24], which is similar to the viscosity of about 50 poise for the borosilicate LAW glass at 1150°C. However, Inconel 690 coupon corrosion tested in the FeP LAW glass at 1150°C showed severe damage, with the coupon failing at the neck region during the test. The Inconel 693 coupon, however, did not show excessive damage during the 1150°C test in the FeP LAW glass. In general, Inconel 693 performed better than Inconel 690 in the corrosion tests with FeP LAW glass, which was also observed in a previous corrosion study [14]. The better performance of Inconel 693 in corrosion tests with the FeP LAW glass is most likely due to the presence of Al_2O_3 in the Inconel 693 alloy that inhibits corrosion. Since part of the Inconel 690 coupon from the1150°C test fell in the melt and damaged the platinum crucible, some of the later tests were conducted in alumina crucibles, as was the case in the earlier study [14]. As is evident from Table 3.2, use of alumina crucible significantly affects the composition of the FeP glass during the test and the results from the test should be used with caution. Tests in alumina crucibles are likely to underestimate the extent of corrosion due to dissolution of Al_2O_3 from the crucible, which changes the composition of the glass during the test.

Inconel 693 was also corrosion tested in the FeP LAW glass at 1050°C and 10A/inch² current density. The coupon after 3 days of testing in the presence of the electric field showed the formation of several secondary phases, including nitrides and phosphides. The reduced phases, such as nitrides and phosphides, were not observed in coupons that were corrosion tested in the FeP glass without an electric field. The formation of secondary phases probably caused expansion of the coupon, making assessment of material loss by measurement of coupon dimensions unreliable. Another important difference between the coupons from tests with and without the electric field is the behavior of Al_2O_3 present in Inconel 693. In corrosion tests on Inconel 693 without an electric field, Al_2O_3 is found in the grain boundaries, potentially inhibiting corrosion, whereas Al_2O_3 is not found in the grain boundaries of the coupons tested in the presence of an electric field.

In summary, reduction of the nominal processing temperature of the FeP glass to 1050°C is certainly advantageous with respect to materials corrosion. However, the catastrophic failure of Inconel 690 in tests at 1150°C, as also observed in a previous study [22] performed with an earlier FeP formulation, would allow little safety margin for that material. Inconel 693 appears to provide significantly better performance in the FeP glass than Inconel 690. However, additional work should be performed, particularly on the effects of electric current, to better understand the evolution over longer periods of time of the alteration phases and morphologies identified in the present work and their consequences for long-term, in-service performance.

The specific heat data for the FeP glass, from 340°C to slightly above the glass transition temperature, varies with temperature in a manner similar to those of two LAW borosilicate glasses previously developed for ORP [25]. The magnitudes of the specific heat values also are similar, expect that the peak specific heat values slightly above the glass transition temperatures were slightly higher $(0.1 - 0.2$ J/g·K higher) for the borosilicate glasses, as compared to the FeP glass. The two LAW borosilicate glasses have glass transition temperatures above 500°C (~520°C and 535°C), while the FeP glass showed a glass transition temperature about 100°C lower (~417°C). In the temperature range above the glass transition temperature, the variation in specific heat with temperature is different for the FeP glass as compared to the two LAW borosilicate glasses [25]. In particular, in that region, the specific heat values for the two LAW borosilicate glasses decrease with temperature, whereas they increase slightly for the FeP glass. The difference in behavior may be due to the heavy crystallization observed in the FeP glass at temperatures somewhat above the glass transition temperature.

Compared to the other waste glasses shown in Figure 4.2, the FeP glass shows densities that are near the high end of the range. However, the change in density with temperature follows a trend that is similar to those of the other glasses. The LAW FeP glass shows density values that are higher than those for the LAW borosilicate glass LAWA44, though both are well below the WTP density limit of 3.7 g/cc at room temperature [26].

The thermal diffusivity and thermal conductivity of the FeP LAW glass are lower than those of WTP borosilicate waste glasses previously studied [25]. The increase in thermal diffusivity and thermal conductivity seen in the properties of the borosilicate glasses, especially above 1000C, is not observed for the FeP glass. This is probably due to foaming suspected in the FeP glass during thermal diffusivity measurement at 1050 and 1075°C, which may have decreased the otherwise rising contribution to thermal diffusivity from radiation. The crystallization observed at temperatures above about 550°C and foaming suspected during thermal diffusivity data collection at 1050 and 1075°C should be noted when using the data on the high temperature properties reported here for the FeP glass melt.

The lower thermal conductivity of the FeP glass would likely translate into slower rates of cooling of filled glass containers (assuming the same geometry). This could have impacts on facility cycle times and the extent of crystallization during container cooling.

SECTION 6.0
REFERENCES

[1] "Glass Formulation and Testing With RPP-WTP LAW Simulants," I.S. Muller, A.C. Buechele, and I.L. Pegg, Final Report, VSL-01R3560-2, Vitreous State Laboratory, The Catholic University of America, Washington, DC, 2/23/01.

[2] "Baseline LAW Glass Formulation Testing," I.S. Muller and I.L. Pegg, Final Report, VSL-03R3460-1, Rev. 0, Vitreous State Laboratory, The Catholic University of America, Washington, DC, 8/8/03.

[3] "Glass Formulations to Support Melter Testing", I.S. Muller and I.L. Pegg, Final Report, VSL-03R3460-2, Rev. 0, Vitreous State Laboratory, The Catholic University of America, Washington, DC, 2/6/04.

[4] "LAW Envelope C Glass Formulation Testing to Increase Waste Loading," K.S. Matlack, W. Gong, I.S. Muller, I. Joseph, and I.L. Pegg, Final Report, VSL-05R5900-1, Rev. 0, Vitreous State Laboratory, The Catholic University of America, Washington, DC, 1/27/06.

[5] "LAW Envelope A and B Glass Formulation Testing to Increase Waste Loading," K.S. Matlack, H. Gan, I.S. Muller, I. Joseph, and I.L. Pegg, Final Report, VSL-06R6900-1, Rev. 0, Vitreous State Laboratory, The Catholic University of America, Washington, DC, 3/23/06.

[6] "Enhanced LAW Glass Formulation Testing," K.S. Matlack, I. Joseph, W. Gong, I.S. Muller, and I.L. Pegg, Final Report, VSL-07R1130-1, Rev. 0, Vitreous State Laboratory, The Catholic University of America, Washington, DC, 10/05/07.

[7] "Glass Formulation Development and DM10 Melter Testing with ORP LAW Glasses," K.S. Matlack, I. Joseph, W. Gong, I.S. Muller, and I.L. Pegg, Final Report, VSL-09R1510-2, Rev. 0, Vitreous State Laboratory, The Catholic University of America, Washington, DC, 6/12/09.

[8] "Waste Loading Enhancements for Hanford LAW Glasses," I.S. Muller, K.S. Matlack, H. Gan, I. Joseph, and I.L. Pegg, Final Report, VSL-10R1790-1, Rev. 0, Vitreous State Laboratory, The Catholic University of America, Washington, DC, 12/1/10.

[9] "Immobilization of Hanford LAW in Iron Phosphate Glasses," C.W. Kim and D.E. Day, Journal of Non-Crystalline Solids, 331, 20-31 (2003).

[10] "Chemically Durable Iron Phosphate Glasses for Vitrifying Sodium Bearing Waste (SBW) Using Conventional and Cold Crucible Induction Melting (CCIM) Techniques," C.W. Kim, C.S. Ray, D. Zhu, D.E. Day, D. Gombert and A. Aloy, Journal of Nuclear Materials, 331, 20-31 (2003).

[11] "Iron Phosphate Glasses as an Alternative Waste Form for Hanford LAW," D-S. Kim, W.C. Buchmiller, M.J. Schweiger, J.D. Vienna, D.E. Day, C.W. Kim, D. Zhu, T.E. Day, T. Neidt, D.K. Peeler, T.B. Edwards, J.A. Reamer and R.J. Workman, PNNL-14251, Pacific Northwest National Laboratory, Richland, WA, (2003).

[12] "Phosphate Glass Development and Demonstration," DOE-EM31 Technology Development and Deployment (TDD) Program Task Plan, WP-5.1.1-2010-001, Rev. 0, 3/31/10.

[13] "Development of Phosphate Glass," H. Gan, and I.L. Pegg, Task Plan (for DOE EM-31 TDD Program Task WP-5.1.1-2010-001), VSL-10E2210-1, Rev. 0, Vitreous State Laboratory, The Catholic University of America, Washington, DC, 09/14/10.

[14] "Corrosion Behavior of Inconel 690 and 693 in an Iron Phosphate Melt," D. Zhu, C.W. Kim and D.E. Day, J. Nucl. Materials, 336, 47-53 (2005).

[15] "Quality Assurance Project Plan for WRPS Support Activities Conducted by VSL," Vitreous State Laboratory, VSL-QAPP-WRPS, Rev. 0, Vitreous State Laboratory, The Catholic University of America, Washington, DC, 3/26/10.

[16] "Master List of Controlled VSL Manuals and Standard Operating Procedures in Use," QA-MLCP, Rev. 60, Vitreous State Laboratory, The Catholic University of America, Washington, DC, 3/21/11.

[17] "Volume-Temperature Relationship in Simulated Glass Forming Nuclear Waste Melts," L.D. Pye, R. Locker and M.H. Plodinec, p. 627-637, in Advances in Materials Characterization, Materials Science Research Vol. 15, Ed. D.R. Rossington, R.A. Condrate and R.L. Snyder, Plenum Press, New York and London (1983).

[18] "Density of $Na_2O-K_2O-CaO-MgO-FeO-Fe_2O_3-Al_2O_3-TiO_2-SiO_2$ Liquids, New Measurements and Derived Partial Molar Properties," R.A. Lange and I.S.E. Carmichael, Geochimica et. Cosmochimica Acta, 51, 2931-2946, (1987).

[19] "Molten Salts Data as Reference Standards for Density, Surface Tension, Viscosity and Electrical Conductivity: KNO_3 and $NaCl$," G. J. Janz, J. Phys. Chem. Ref. Data 9, 791-829 (1980).

[20] L.P. Phyllipov, Temperature Wave Techniques, Compendium of Thermophysical Property Measurement Methods, Vol. 1, Survey of Measurement Techniques, ed. K.D. Maglić, A. Cezairliyan, and V.E. Peletsky, Plenum Press, New York and London (1984).

[21]   "A Method for the Measurement of Thermal Diffusivity of Molten Glass," A.F. Van Zee and C.L. Babcock, J. Am. Ceramic Soc., 34, 244-250 (1951).

[22]   "Inconel 690 Corrosion in WTP HLW Glass Melts Rich in Aluminum, Bismuth, Chromium or Aluminum/Sodium," Z. Feng, H. Gan, and I.L. Pegg, Final Report, VSL-08R1370-1, Rev. 0, Vitreous State Laboratory, The Catholic University of America, Washington, DC, 9/23/08.

[23]   "RPP-WTP High Temperature LAW Materials Assessment," I. Vidensky, M. Chaudhuri, H. Gan, G. Diener, L. Andre, R.K. Mohr and I.L. Pegg, Final Report, VSL-04R4950-1, Rev. 0, Vitreous State Laboratory, The Catholic University of America, Washington, DC, 1/14/05.

[24]   "Iron Phosphate Glass Development and Demonstration," D. E. Day and D.K. Peeler, Presentation at the DOE-EM Environmental Management Technical Exchange, Atlanta, GA, 11/17/10.

[25]   "Crystal Settling, Redox and High Temperature Properties of ORP HLW and LAW Glasses," H. Gan, I. S. Muller, D. A. McKeown, M. Chaudhuri, Z. Feng, C. Viragh, C. Wang, R. Cecil, W. Zhao, W.K. Kot, I. Joseph and I.L. Pegg, Final Report, VSL-09R1510-1, Rev. 0, Vitreous State Laboratory, The Catholic University of America, Washington, DC, 6/18/09.

[26]   U.S. Department of Energy, Office of River Protection, "Design, Construction, and Commissioning of the Hanford Tank Waste Treatment and Immobilization Plant," Contract Number: DE-AC27-01RV14136, 2001; and subsequent amendments.

Table 2.1. Target and Analyzed Compositions (wt%) of the FeP Glass Used in Corrosion Tests.

Oxide	Target (wt%)	XRF (wt%)
Al_2O_3	13.21	11.71
B_2O_3*	0.03	0.03
Bi_2O_3	1.77	1.99
CaO	1.06	1.13
Cl	0.04	0.062
CoO	-	0.005
Cr_2O_3	2.70	3.26
Cs_2O	0.13	0.19
CuO	-	0.006
F*	0.16	-
Fe_2O_3	7.10	7.55
HfO_2	-	0.014
K_2O	0.78	0.83
La_2O_3	0.71	0.76
MnO	-	0.009
Na_2O	20.03	20.76
P_2O_5	38.06	38.13
Pt	-	0.005
Re_2O_7	0.03	0.017
SO_3	4.37	3.56
SiO_2	5.58	5.39
SnO_2	-	0.003
TiO_2	-	0.005
ZnO	3.55	3.80
ZrO_2	0.71	0.76
Total	100.02	99.98

*Target; value not determined by XRF
- Empty data field

Table 2.2. Corrosion Test Conditions and Sample Identifications.

Alloy	Glass ID after 7-day Corrosion	Glass ID after 14-day Corrosion	Metal Coupon ID after Corrosion	Test Conditions
Inconel 690	FeP1050-1	-	INC690-FeP1050	7 days at 1050°C
Inconel 693	FeP1050-2	-	INC693-FeP1050	
Inconel 690	FeP1100-1	-	INC690-FeP1100	7 days at 1100°C
Inconel 693	FeP1100-2	-	INC693-FeP1100	
Inconel 690	FeP1150-1	-	INC690-FeP1150[*]	7 days at 1150°C
Inconel 693	FeP1150-2	-	INC693-FeP1150	
Inconel 690	FeP1050-3	FeP1050-5	INC690-FeP1050-2	7 days at 1050°C, replace with new glass, continue for 7 more days
Inconel 693	FeP1050-4	FeP1050-6	INC693-FeP1050-2	
INCONEL 693 (Pin)	FeP1050EC[#]	-	INC693EC-1050-A (1.5 mm from tip)	3 days at 1050°C with 10 A/in^2 current density
			INC693EC-1050-B (5 mm from tip)	
			INC693EC-1050-C (9 mm from tip)	

- Empty data field
[*] Coupon failed at neck region during test
[#] After 3-day electrical corrosion test

Table 3.1. Results of Metal Corrosion Tests.

Metal Coupon ID after Corrosion	Test Conditions	Neck Loss (mil)	Half Down Loss (mil)	Scale Thickness (μm)	Grain Boundary Damage Depth$ (μm)	Maximum Cr Depletion Depth (μm)	% Cr Loss at Coupon Surface
INC690-FeP1050	7 days at 1050°C	0	0	20	70	100	27
INC693-FeP1050		<0.5	1	20	200	100	8.4
INC690-FeP1100	7 days at 1100°C	0	0	40	175	250	40
INC693-FeP1100		0.5	1.5	15	350	200	20
INC690-FeP1150#	7 days at 1150°C	NA	NA	NA	NA	NA	NA
INC693-FeP1150		<0.5, 2*	<0.5, 2*	80	40	300	10
INC690-FeP1050-2	7 days at 1050°C, replace with new glass, continue for 7 more days	0	0	Lost in mounting	125	250	30
INC693-FeP1050-2		0	0	30	200	325	8
INC693EC-1050-A (1.5 mm from tip)	3 days at 1050°C with 10 A/in² current density	0**	NA	20-60	350	200	30
INC693EC-1050-B (5 mm from tip)		0**	NA	0-100	350	220	43
INC693EC-1050-C (9 mm from tip)		2**	NA	30-150	350	180	33

Coupon failed at neck region during test; * Based on pre-test coupon dimensions; ** Dimension loss at point of sectioning which is not neck area; values of zero are misleading because of expansion of coupon $ From examination of SEM at half down region, or at point of sectioning.

**Table 3.2. XRF Analyzed Compositions (wt%) of FeP Glasses
after Corrosion Tests.**

Oxide	Original Glass Target	Original Glass XRF	FeP1050-1	FeP1050-2	FeP1050-3 (Al_2O_3 crucible)	FeP1050-4	FeP1050-5 (Al_2O_3 crucible)
Al_2O_3	13.21	11.71	12.81	12.70	15.21	12.31	15.26
B_2O_3*	0.03	0.03	0.03	0.03	0.03	0.03	0.03
Bi_2O_3	1.77	1.99	1.74	1.79	2.16	2.09	2.12
CaO	1.06	1.13	1.10	1.12	1.23	1.20	1.21
Cl	0.04	0.06	-	-	-	0.00	-
CoO	-	0.01	0.01	-	0.00	-	-
Cr_2O_3	2.70	3.26	2.44	2.73	0.86	2.35	1.07
Cs_2O	0.13	0.19	0.12	0.16	0.19	0.19	0.18
CuO	-	0.01	-	-	-	-	-
F*	0.16	-	-	-	-	-	-
Fe_2O_3	7.10	7.55	6.83	7.08	6.67	7.62	6.80
HfO_2	-	0.01	0.02	0.01	0.03	0.03	0.03
K_2O	0.78	0.83	0.80	0.81	0.88	0.86	0.87
La_2O_3	0.71	0.76	0.75	0.75	0.86	0.81	0.80
MnO	-	0.01	0.01	0.02	0.02	0.02	0.02
Na_2O	20.03	20.76	22.15	22.28	19.46	21.04	19.85
NiO	-	-	-	0.01	-	0.00	-
P_2O_5	38.06	38.13	40.42	39.71	40.57	40.02	40.23
Pt	-	0.01	0.01	0.01	0.01	0.01	0.01
Re_2O_7	0.03	0.02	-	-	0.01	0.01	0.01
SO_3	4.37	3.56	1.09	1.01	1.67	0.96	1.60
SiO_2	5.58	5.39	5.62	5.55	5.61	5.59	5.52
SnO_2	-	0.00#	0.00	0.00	-	-	-
TiO_2	-	0.01	-	0.01	0.01	0.02	0.01
ZnO	3.55	3.80	3.42	3.53	3.69	4.01	3.60
ZrO_2	0.71	0.76	0.62	0.65	0.79	0.77	0.76
Sum	100.0	100.0	100.0	100.0	100.0	100.0	100.0

* Targets; values not determined by XRF.

- Empty data field; components are present at concentrations less than 0.005 wt%

Table 3.2. XRF Analyzed Compositions (wt%) of FeP Glasses after Corrosion Tests (cont'd).

Oxide	Original Glass Target	Original Glass XRF	FeP1050-6	FeP1100-1 (Al$_2$O$_3$ crucible)	FeP1100-2	FeP1150-2	FeP1050EC
Al$_2$O$_3$	13.21	11.71	12.04	17.06	12.60	12.41	12.20
B$_2$O$_3$*	0.03	0.03	0.03	0.03	0.03	0.03	0.03
Bi$_2$O$_3$	1.77	1.99	1.87	1.95	1.91	2.05	1.67
CaO	1.06	1.13	1.13	1.16	1.17	1.19	1.07
Cl	0.04	0.06	-	-	-	-	0.03
CoO	-	0.01	-	0.00	-	0.00	0.00
Cr$_2$O$_3$	2.70	3.26	2.82	0.30	2.14	2.49	2.40
Cs$_2$O	0.13	0.19	0.14	0.17	0.19	0.16	0.18
CuO	-	0.01	-	-	-	-	-
F*	0.16	-	-	-	-	-	-
Fe$_2$O$_3$	7.10	7.55	7.32	6.53	7.21	7.72	6.59
HfO$_2$	-	0.01	0.02	0.03	0.02	0.03	0.02
K$_2$O	0.78	0.83	0.84	0.84	0.83	0.85	0.79
La$_2$O$_3$	0.71	0.76	0.76	0.79	0.77	0.80	0.69
MnO	-	0.01	0.01	0.02	0.02	0.02	-
Na$_2$O	20.03	20.76	20.66	20.93	21.94	21.36	21.93
NiO	-	-	-	-	0.01	0.01	0.01
P$_2$O$_5$	38.06	38.13	41.17	39.95	40.43	39.90	40.21
Pt	-	0.01	0.01	0.01	0.01	0.01	-
Re$_2$O$_7$	0.03	0.02	-	-	-		0.01
SO$_3$	4.37	3.56	1.15	0.87	0.56	0.25	2.76
SiO$_2$	5.58	5.39	5.64	5.60	5.71	5.95	5.49
SnO$_2$	-	0.00	-	-	0.00	0.00	-
TiO$_2$	-	0.01	0.01	0.01	0.01	0.01	0.01
ZnO	3.55	3.80	3.66	3.04	3.70	3.97	3.29
ZrO$_2$	0.71	0.76	0.66	0.71	0.72	0.76	0.60
Sum	100.0	100.0	100.0	100.0	100.0	100.0	100.0

* Targets; values not determined by XRF.

- Empty data field; components are present at concentrations less than 0.005 wt%

Table 4.1. Specific Heat of FeP Glass.

Data Collected on Heating		Interpolated Values		Data Collected on Cooling	
Temperature (°C)	Specific Heat (J/g·K)	Temperature (°C)	Specific Heat (J/g·K)	Temperature (°C)	Specific Heat (J/g·K)
340	1.025	550	1.235	730	1.297
350	1.036	560	1.238	740	1.296
360	1.042	570	1.242	750	1.296
370	1.036	580	1.246	760	1.296
380	1.050	590	1.249	770	1.288
390	1.068	600	1.253	780	1.294
400	1.085	610	1.256	790	1.288
410	1.129	620	1.260	800	1.298
420	1.210	630	1.264	810	1.294
430	1.341	640	1.267	820	1.296
440	1.420	650	1.271	830	1.297
450	1.423	660	1.275	840	1.302
460	1.393	670	1.278	850	1.305
470	1.362	680	1.282	860	1.310
480	1.310	690	1.285	870	1.311
490	1.256	700	1.289	880	1.316
500	1.241	720	1.296	890	1.314
510	1.237	-	-	900	1.309
520	1.237	-	-	910	1.315
530	1.232	-	-	920	1.313
540	1.231	-	-	930	1.310
-	-	-	-	940	1.309
-	-	-	-	950	1.308
-	-	-	-	960	1.300
-	-	-	-	970	1.306
-	-	-	-	980	1.306
-	-	-	-	990	1.306
-	-	-	-	1000	1.310
-	-	-	-	1010	1.317

- Empty data field

Table 4.2. Density of FeP Melt.

Temperature (°C)	Density (g/cm^3)
800	2.550
900	2.534
1000	2.502
1050	2.483
1075	2.475

Table 4.3. Thermal Diffusivity of FeP Melt (Heat wave period - 7200 seconds).

T (°C)	Thermal Diffusivity (cm^2/s)
800	0.002505
900	0.002477
1000	0.002504
1050*	0.002392
1075*	0.002344

* Foaming suspected during measurement

Table 4.4. Calculation of Thermal Conductivity from Thermal Diffusivity, Density, and Heat Capacity of FeP Melt.

Temperature (^{o}C)	Thermal Diffusivity* (cm^2/s)	Density (g/cm^3)	Heat Capacity (J/K.g)	Thermal Conductivity (J/cm.s.K)	Thermal Conductivity (Cal/cm.s.K)
800	0.002495	2.550	1.298	0.008261	0.001974
900	0.002495	2.534	1.309	0.008277	0.001978
1000	0.002495	2.502	1.310	0.008175	0.001954
1050	0.002495	2.483	1.310	0.008112	0.001939
1075	0.002495	2.475	1.310	0.008088	0.001933

* Average value of thermal diffusivities at 800, 900 and 1000°C

2"

0.15"

Section line

0.30"
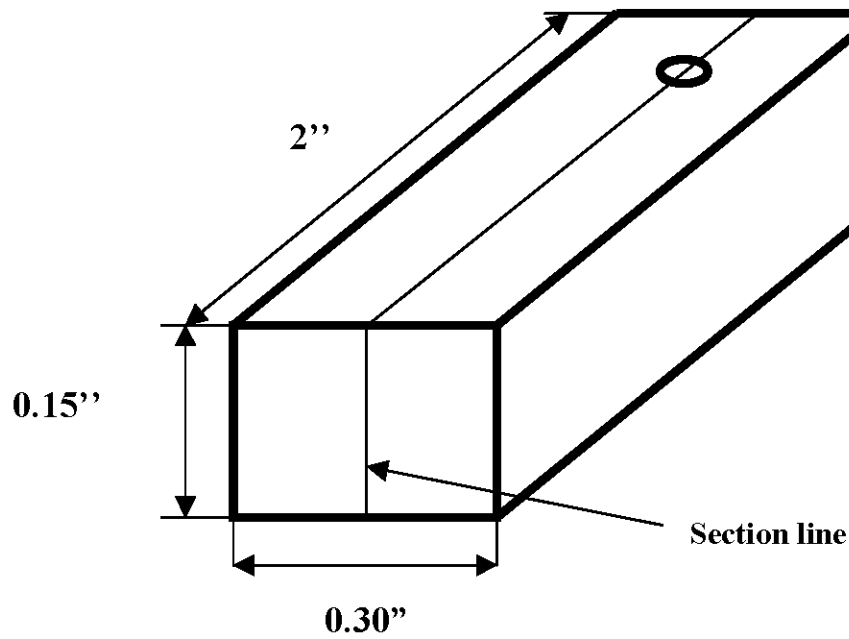
Figure 2.1. Schematic diagram of a metal coupon showing typical dimensions and line indicating where the coupon is sectioned after testing.
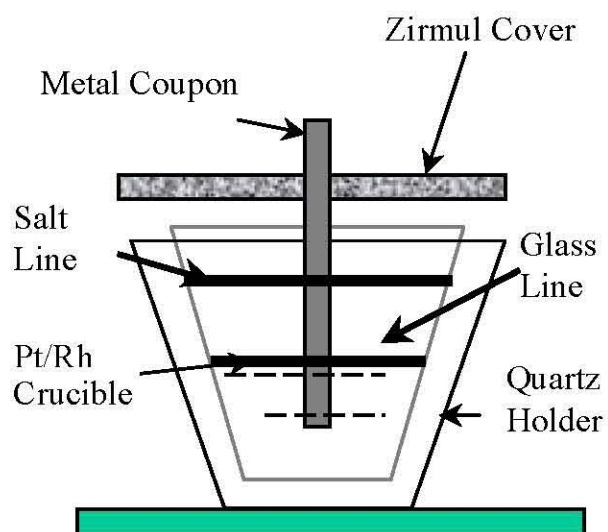
Figure 2.2. Experimental setup for metal coupon corrosion tests. Note: No salt phase was present in the present tests so the salt line is not relevant.
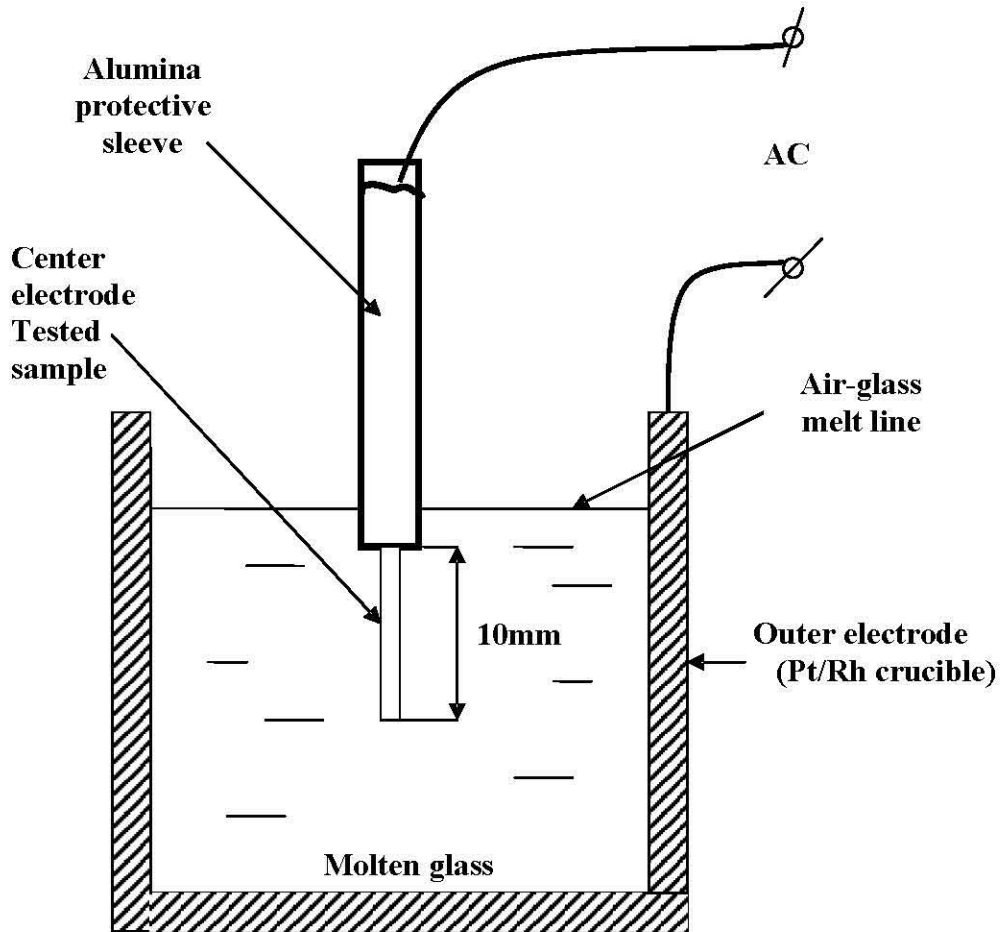
Figure 2.3. Test setup for the electrical corrosion experiments.
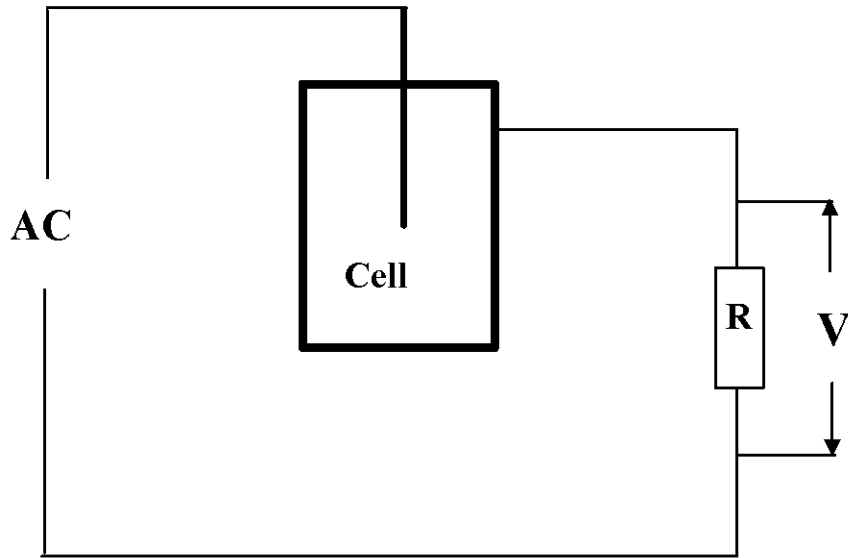
Figure 2.4. Electrical circuit for the corrosion tests.
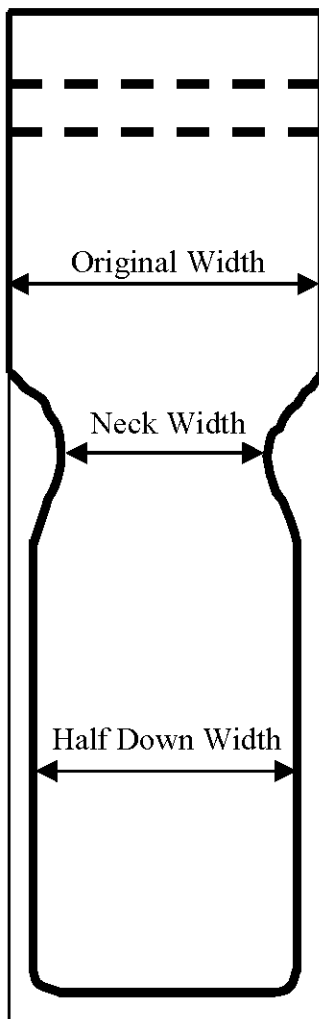
Figure 2.5. Schematic diagram of the cross section of a reacted metal coupon after a typical glass contact corrosion test. Measured widths do not include any scale.
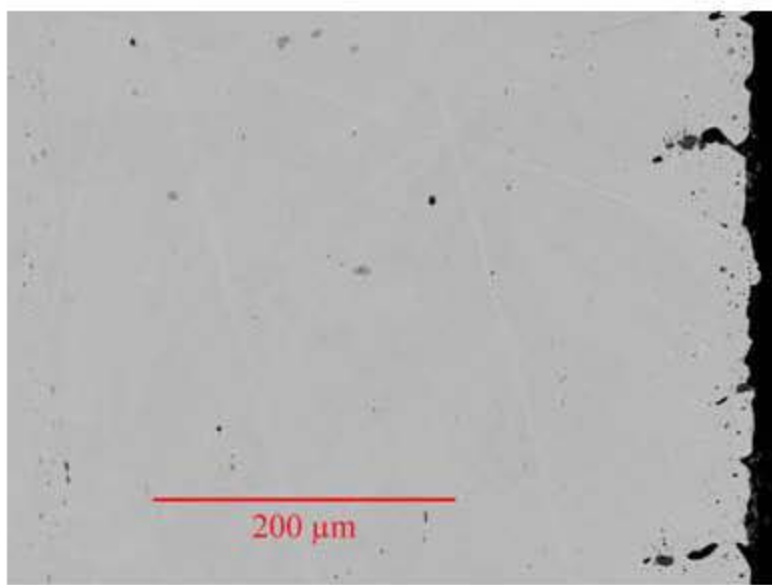
a) Cross section near coupon surface
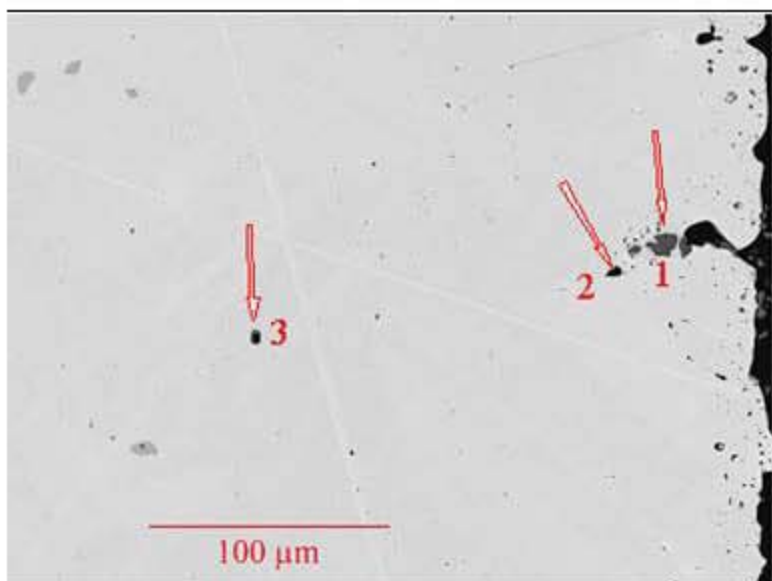
b) Metal near surface

1: Cr_2O_3, 2: Al_2O_3, 3: MgO containing a trace of Ti (probably an impurity in the original Inconel 690).

Figure 3.1. Micrographs of INC690-FeP1050 (Inconel 690, 7 days at 1050°C).
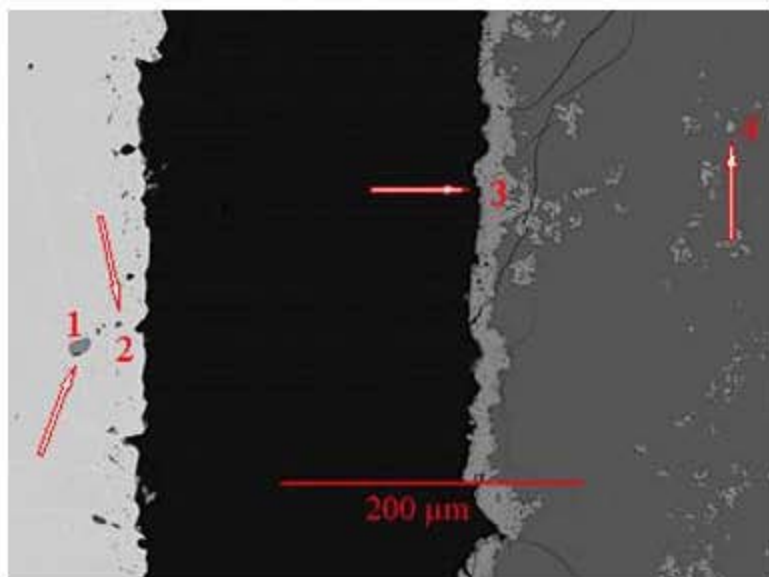
c) Metal near surface
1: Cr_2O_3 containing traces of Ti and Al, 2: Al_2O_3, 3: Cr_2O_3 containing a trace of Fe,
4: Chromite spinel

**Figure 3.1. Micrographs of INC690-FeP1050 (Inconel 690, 7 days at 1050°C) (cont'd).**
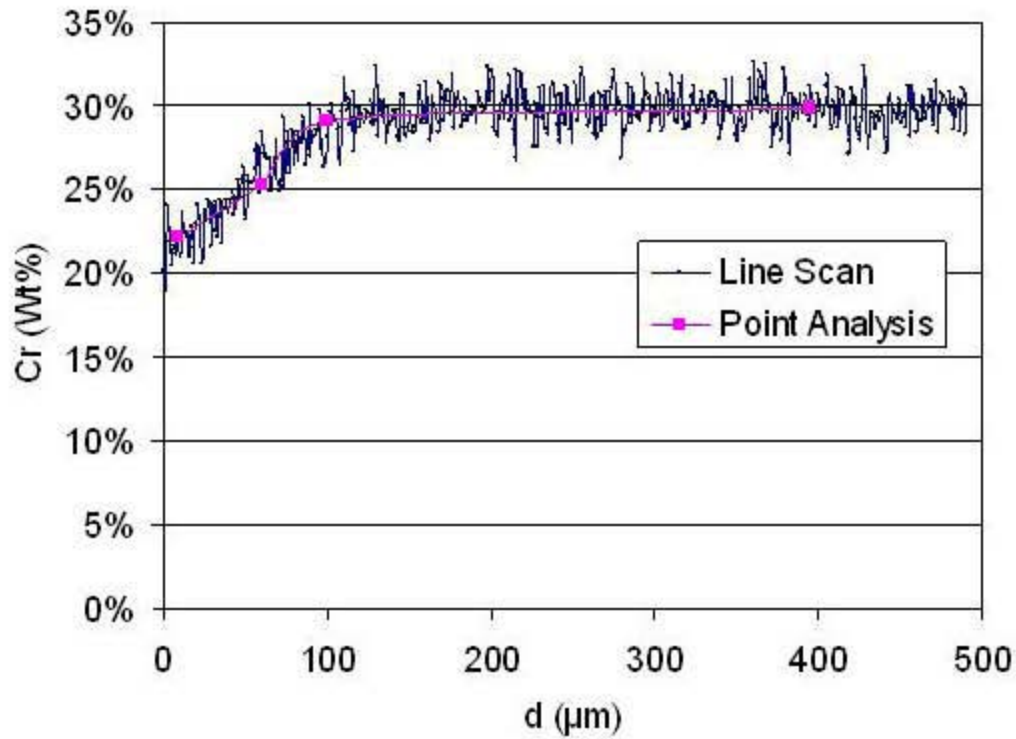
**Figure 3.2. Cr concentration profile in coupon INC690-FeP1050 (Inconel 690 in FeP glass at 1050°C for 7 days). Cr depletion is based on the SEM X-ray line scan into the coupon near the half-down area. Point analyses were done and are overlaid on the curve to calibrate concentration. The Cr depletion depth is about 100 μm.**
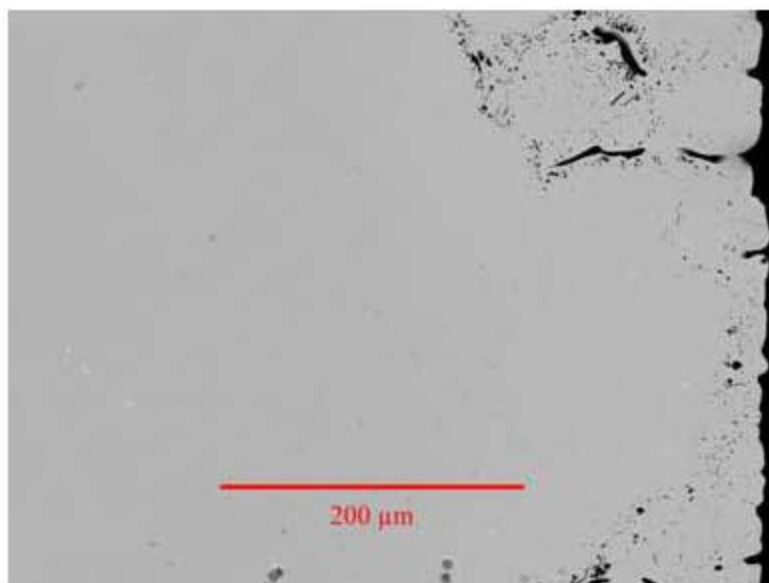
a) Coupon cross section near surface
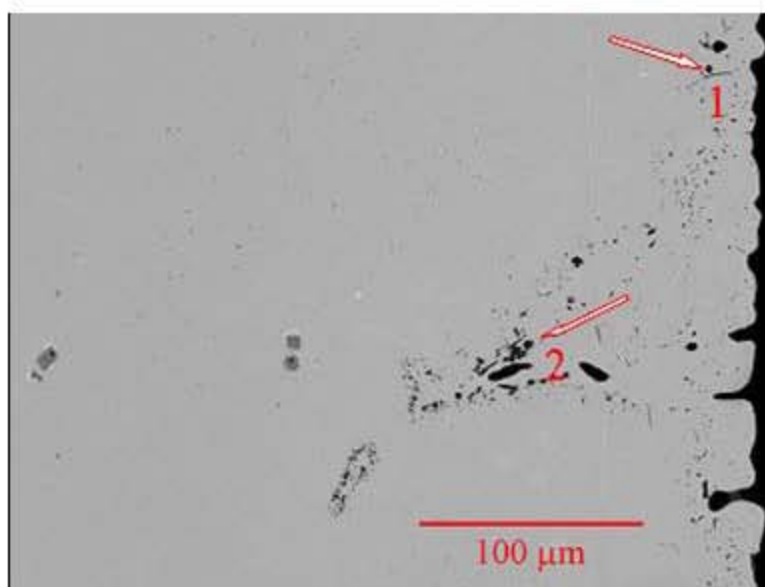
b) Metal near surface

1, 2: Al_2O_3. Several inclusions present in the original Inconel 693 and not corrosion products are also evident in the micrograph. The three dark grey spots to the left of arrow 2 are Ti containing traces of Zr and occasionally Nb. The small bright spot in the center of the micrograph is mostly Zr with some Ti.

Figure 3.3. Micrographs of INC693-FeP1050 (Inconel 693, 7 days at 1050°C).
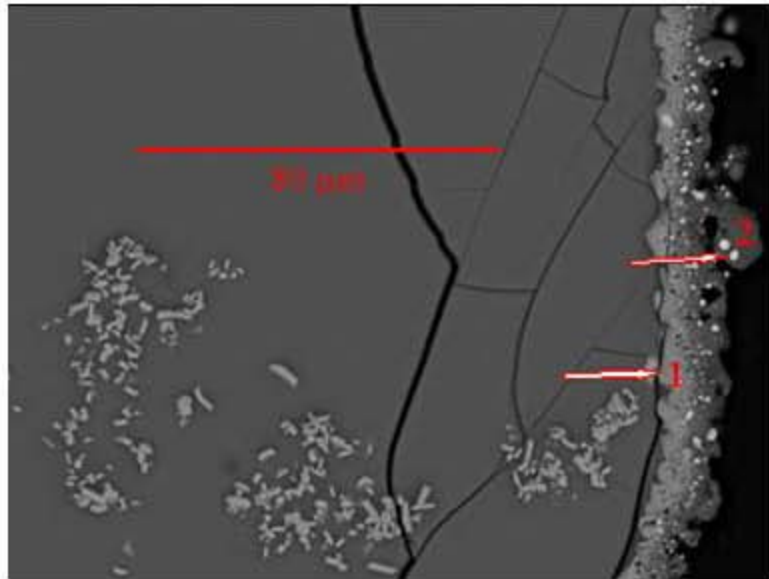
c) Detached scale with adherent glass

Scale (to right) detached from coupon and adherent glass (to left). 1: Cr_2O_3 containing Fe and Al, 2: Complex Ni, Fe, Cr, P, Al, O-containing region; probably metallic, mostly reduced material. Inner (to right) dark layer on scale surrounding the bright spot appears to be high alumina Cr_2O_3-Al_2O_3 solid solution.

Figure 3.3. Micrographs of INC693-FeP1050 (Inconel 693, 7 days at 1050°C) (cont'd).
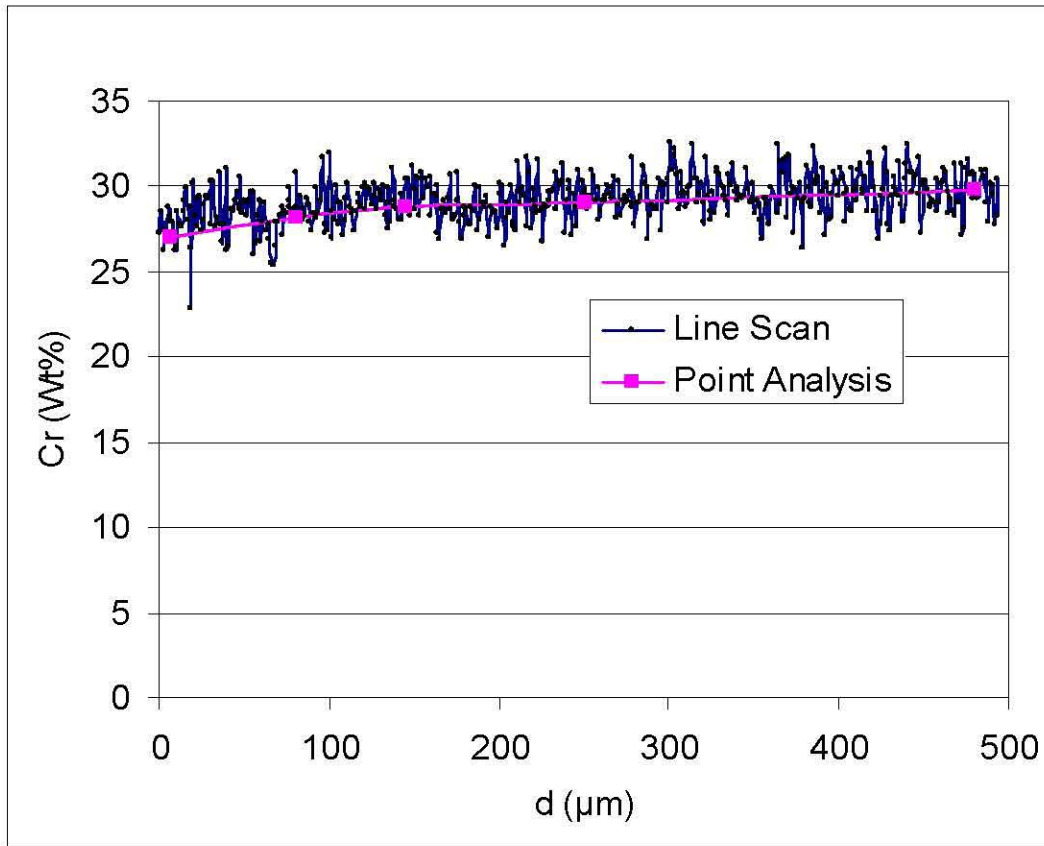
Figure 3.4. Cr concentration profile in coupon INC693-FeP1050 (Inconel 693 in FeP glass at 1050°C for 7 days). Cr depletion is based on the SEM X-ray line scan into the coupon near the half-down area. Point analyses were done and are overlaid on the curve to calibrate concentration. The slope of the curve is small, but point analyses indicate a Cr depletion depth of about 100 μm.
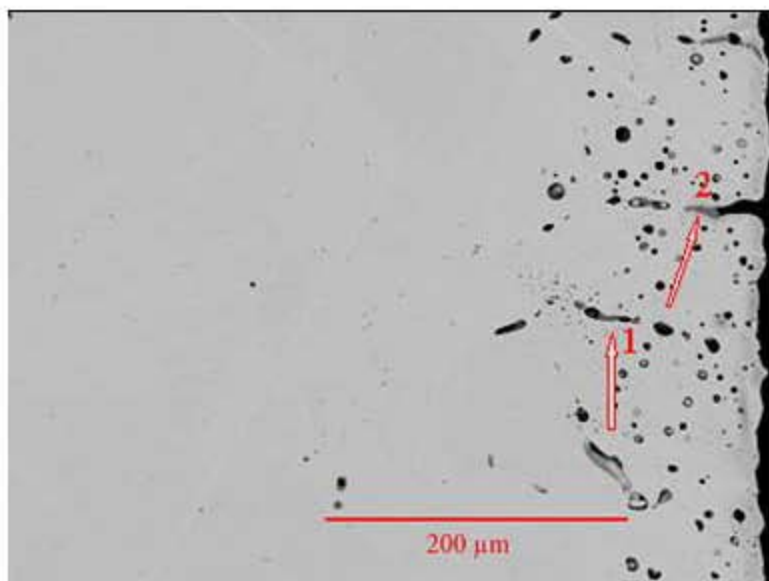
a) Coupon near the half-down region
1: TiO_2, 2; Cr_2O_3 incorporating some Ti
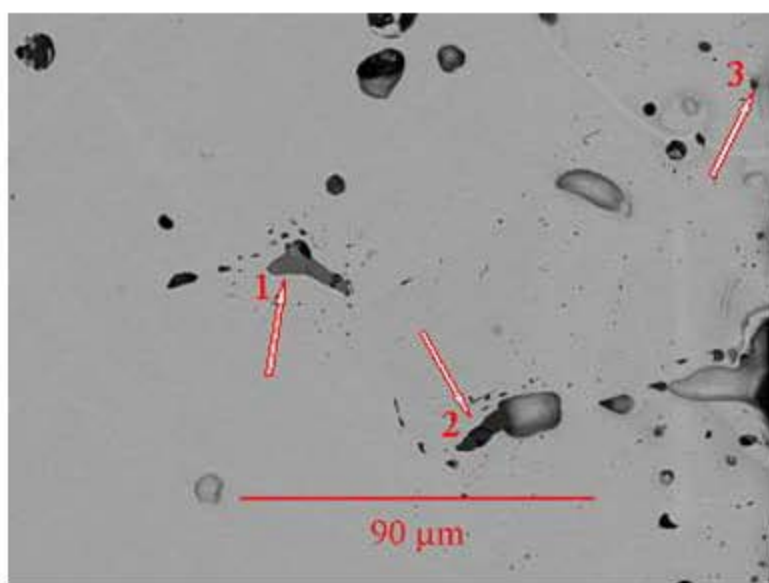
b) Coupon near the half-down region
1: TiO_2, 2: Al_2O_3 with some Zr and Si, 3: Al_2O_3 with trace of silica.

Figure 3.5. Micrographs of INC690-FeP1100 (Inconel 690, 7 days at 1100°C).
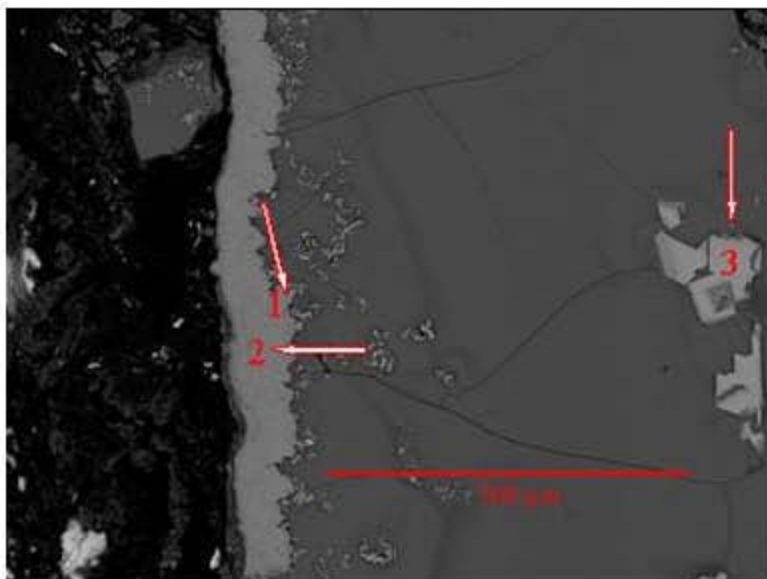
c) Cross section of the detached scale
1: Fe-Cr spinel (high Cr), 2: Cr_2O_3, 3: Fe, Zn-Cr spinel (zincochromite with some Fe substituting for Cr).

Figure 3.5. Micrographs of INC690-FeP1100 (Inconel 690, 7 days at 1100°C) (cont'd).
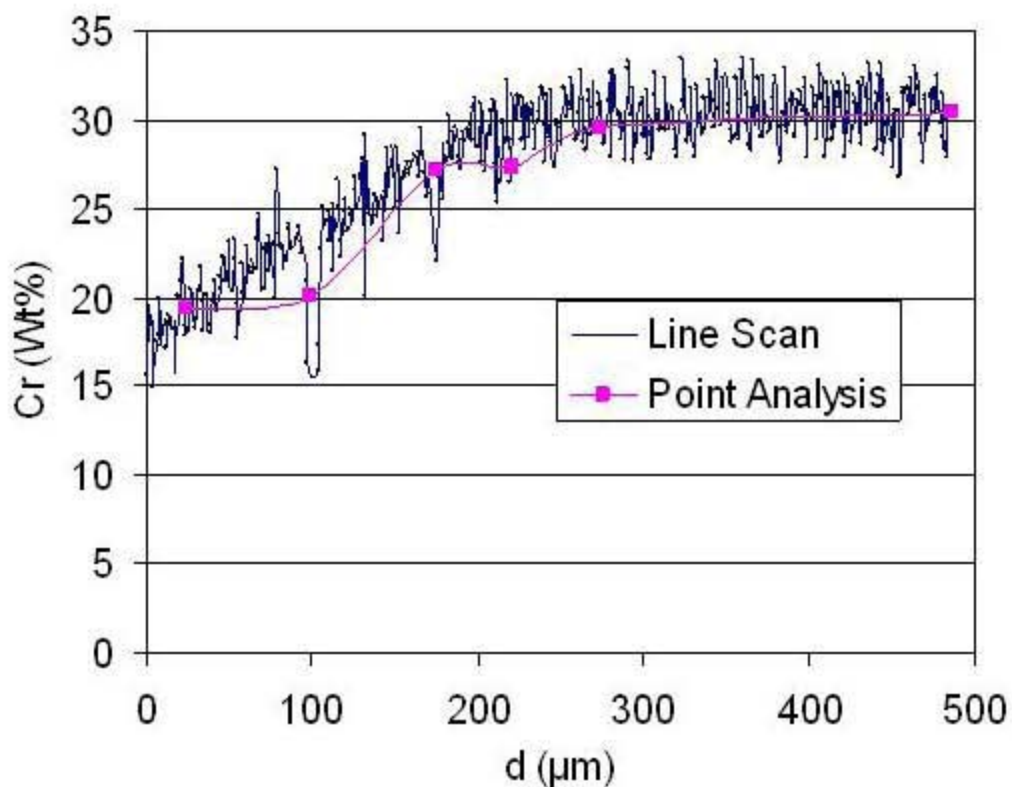
Figure 3.6. Cr concentration profile in coupon INC690-FeP1100 (Inconel 690 in FeP glass at 1100°C for 7 days). Cr depletion is based on the SEM X-ray line scan into the coupon near the half-down area. Point analyses were done and are overlaid on the curve to calibrate concentration. The Cr depletion depth is about 250 μm.
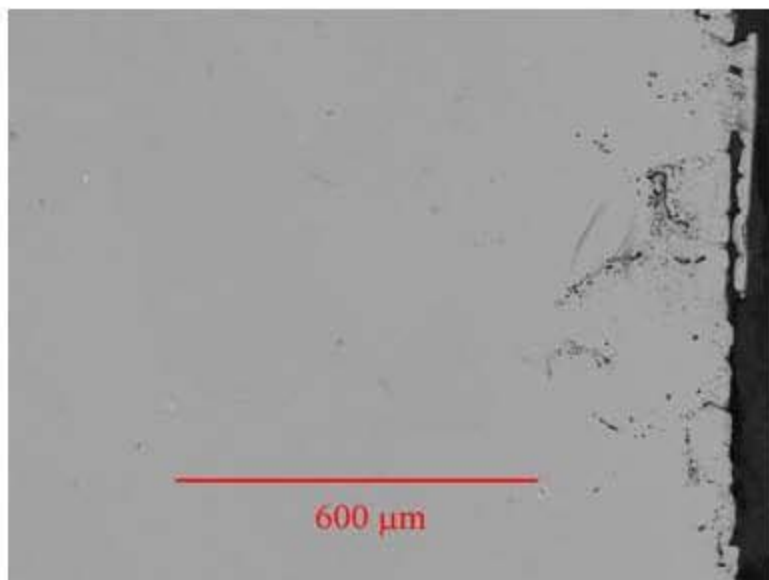
a) Coupon cross section near half down region.
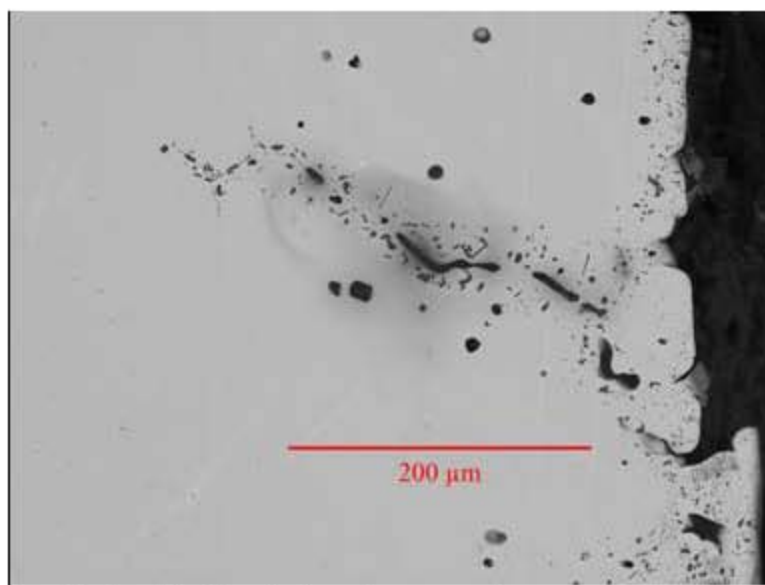
b) Detail of grain boundary attack.

Figure 3.7. Micrographs of INC693-FeP1100 (Inconel 693, 7 days at 1100°C).
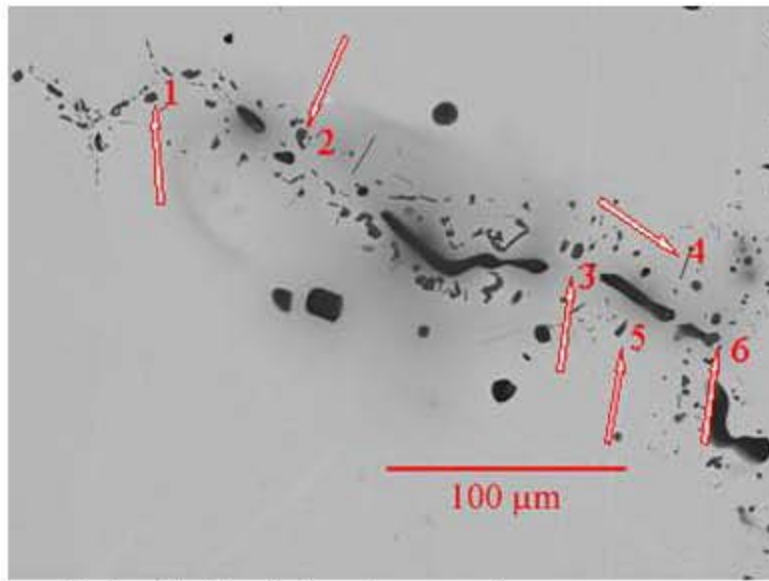
c)   Detail of grain boundary attack

Detail of b) above. 1, 2, 3, 4 5 and 6 are all Al_2O_3 phases containing small amounts of silica. Pockets of pure silica are sometimes found in the linear grain boundary regions.

d)   Detached scale with adherent glass

1, 2 are Fe-Cr-Al spinel. Bright spots in the metal contact scale at the right are metallic residue of corroded Inconel containing varying amounts of phosphorus, probably as phosphide.

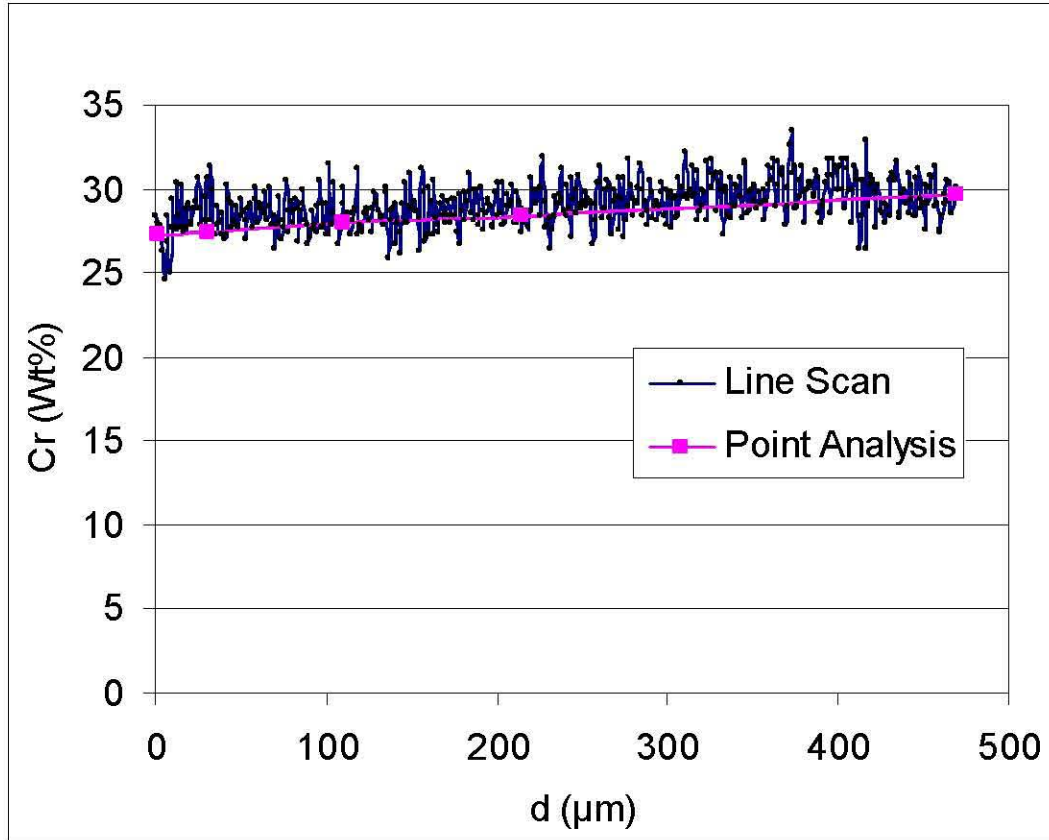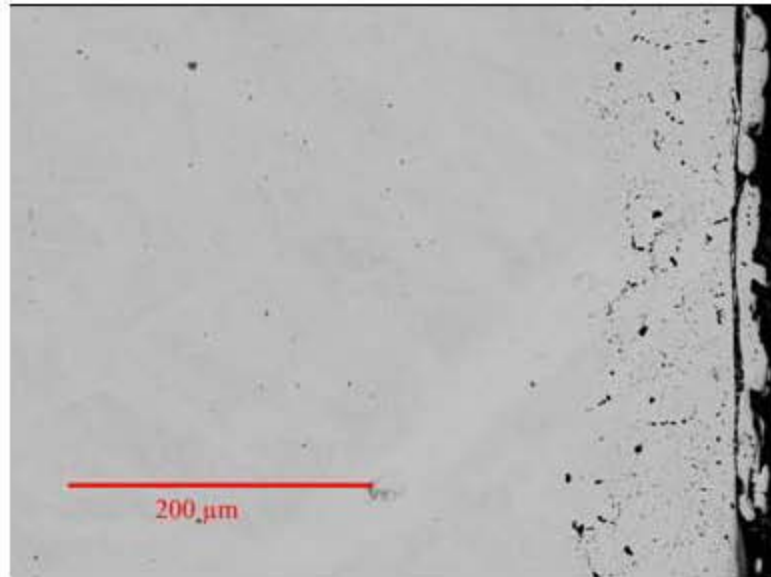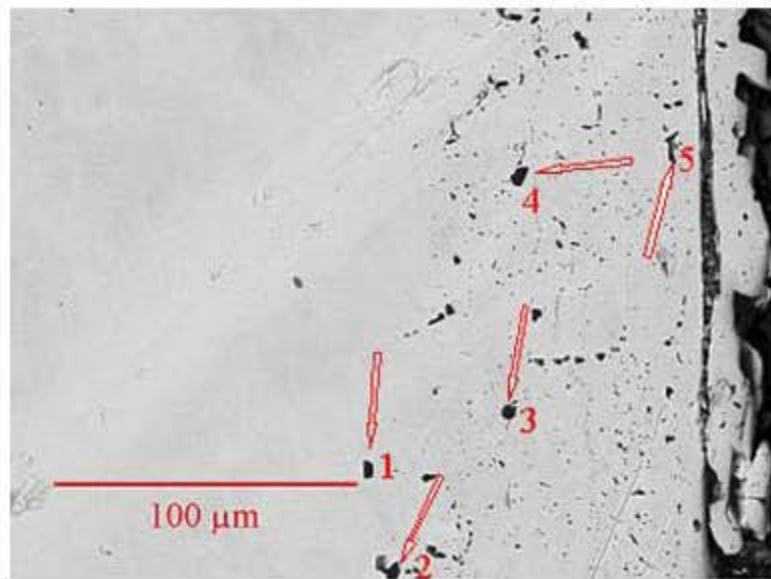**Figure 3.7. Micrographs of INC693-FeP1100 (Inconel 693, 7 days at 1100°C) (cont'd).**
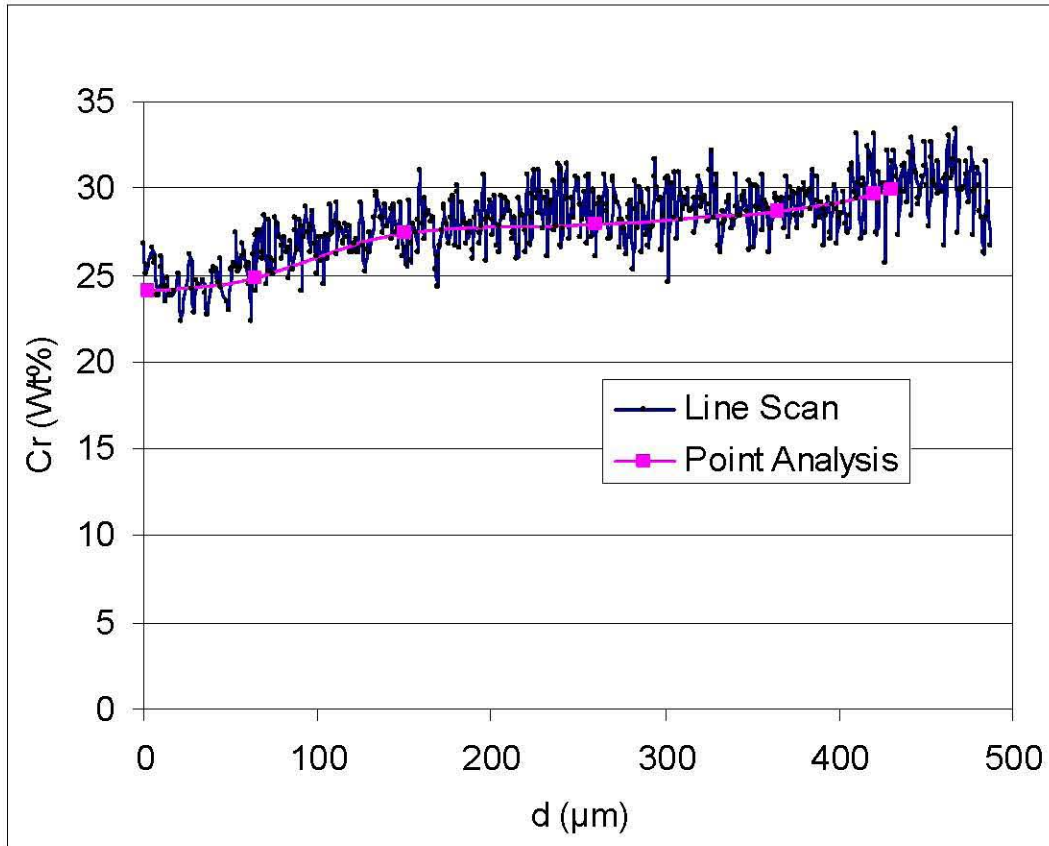
Figure 3.8. Cr concentration profile in coupon INC693-FeP1100 (Inconel 693 in FeP glass at 1100°C for 7 days). Cr depletion is based on the SEM Cr line scan done near the half-down area. The Cr depletion profile actually seems to have two segments. The first segment starts at about 400 μm and proceeds with a small slope to about 200 μm from the surface where its slope increases. The Cr depletion depth is reported in the results as 200 μm.
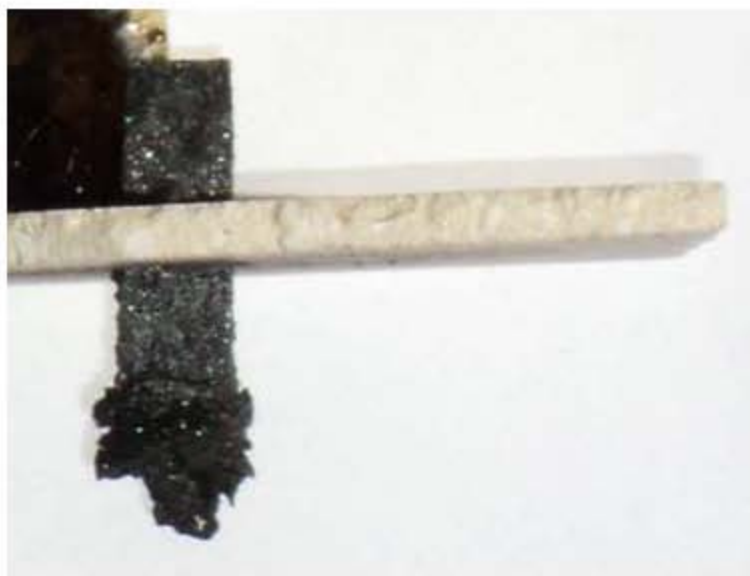
a) The damaged Inconel 690 coupon still mounted to Zurmul ceramic cover.
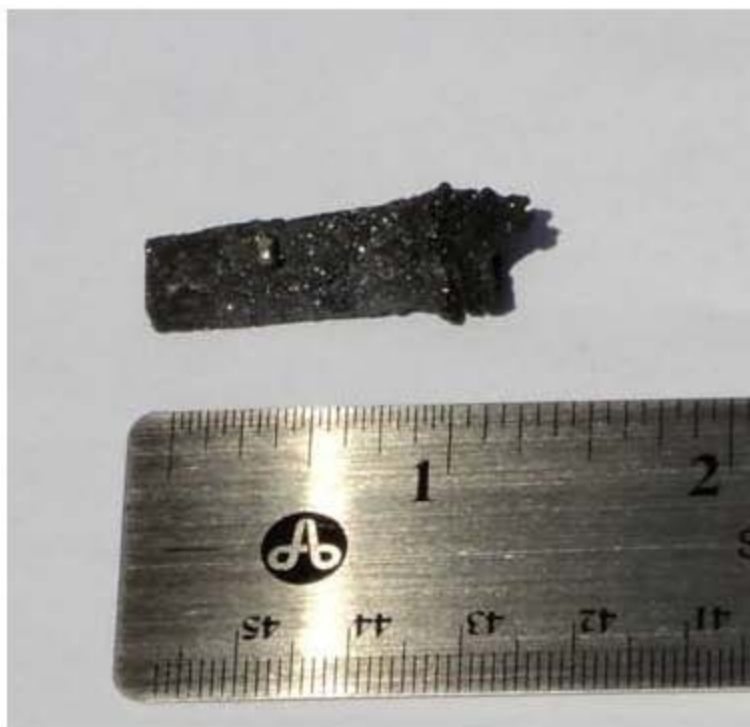
b) Damaged Inconel 690 coupon next to ruler for size reference.

Figure 3.9. Images of damaged INC690-FeP1150 (Inconel 690, 1150°C for 7 days).

c) The damaged Inconel 690 coupon cross sectioned after mounting in epoxy.
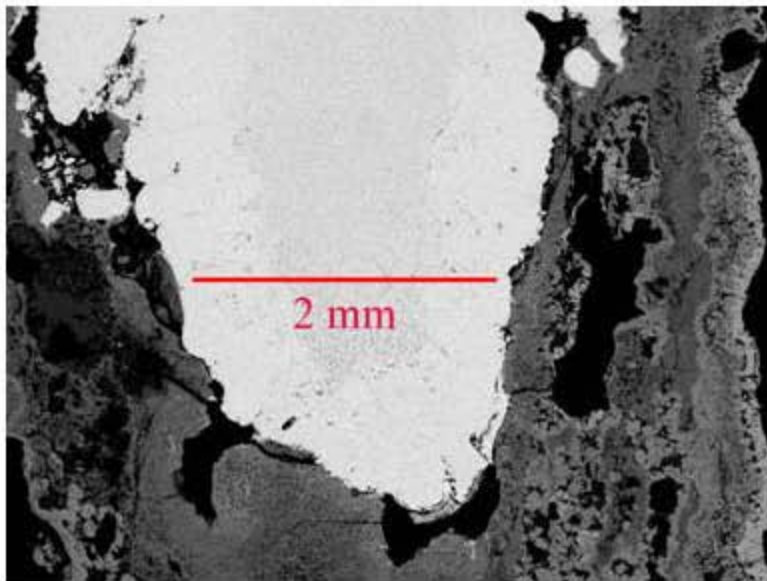
d) SEM micrograph of the cross section through the lower tip area of the remaining upper portion of coupon INC690-FeP1150 and its adherent scale. This region constituted the upper neck area at the time of coupon failure. The brighter area about 800 μm wide around the perimeter of the tip is the region of greatest Cr depletion.

Figure 3.9. Images of damaged INC690-FeP1150 (Inconel 690, 1150°C for 7 days) (cont'd).
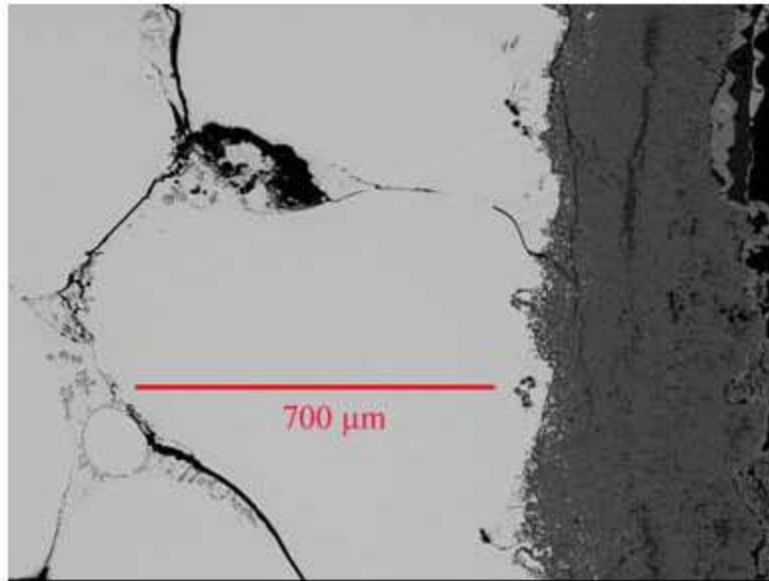
e) SEM micrograph of the cross section of the scale-coupon interface in the tip area of coupon INC690-FeP1150 showing the cracking caused by grain boundary attack and metal loss. The round nodule at the junction of the three cracks in the lower left of the micrograph is surrounded by extensive dendritic CrS crystallization.
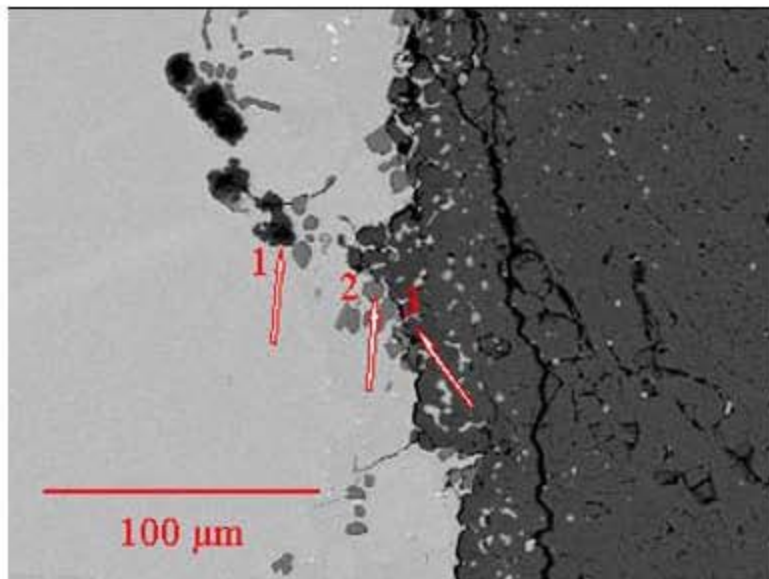
f) SEM micrograph detailing an attacked area at the metal-scale interface of coupon INC690-FeP1150. Bright spots in remaining metal at top-center of micrograph are bismuth. Arrows 1, 3 locate Cr_2O_3-Al_2O_3 solid solution (Cr-rich); arrow 2 locates CrS.

Figure 3.9. Images of damaged INC690-FeP1150 (Inconel 690, 1150°C for 7 days) (cont'd).
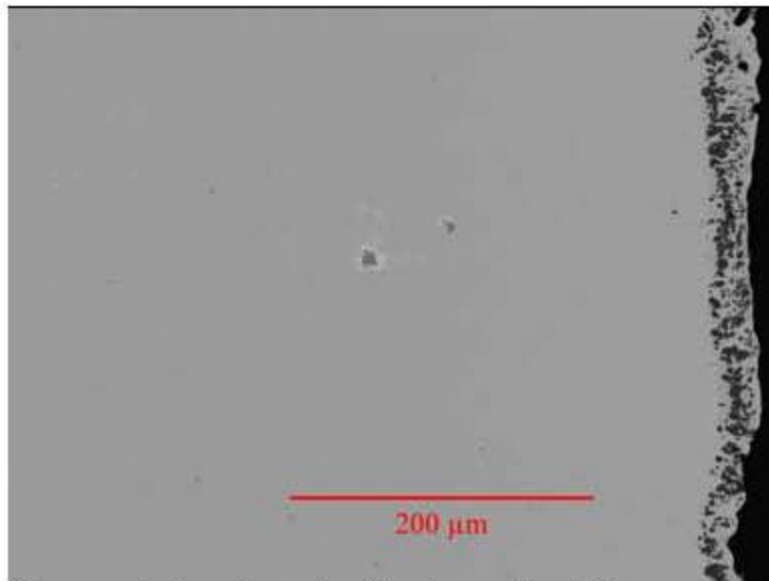
a) Micrograph showing subsurface layer of nodules
    The grey spots with a lighter rim in the center of the micrograph are an
    occasionally seen non-uniformity in the original Inconel, Ti surrounded by
    Nb-Zr.
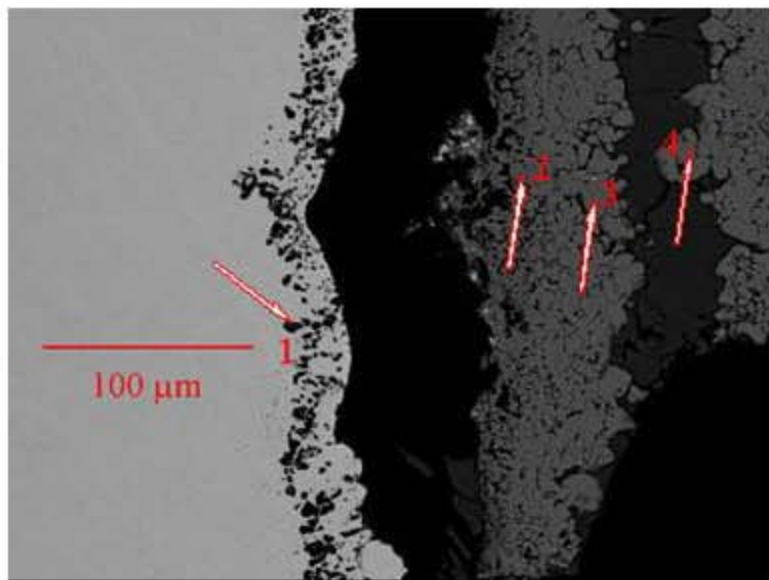
b) Details of nodules from a)
    1: Al_2O_3. 2, 3, and 4: Cr_2O_3 containing a small amount of Fe-Cr-Al spinel.

Figure 3.10. Micrographs of INC693-FeP1150 (Inconel 693, 7 days at 1150°C).
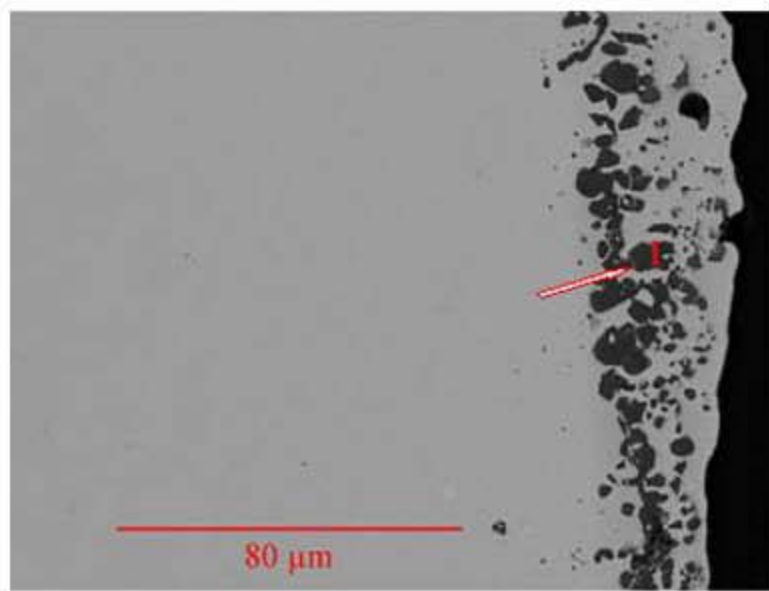
c) SEM micrograph detailing the surface attack
1: Al_2O_3

Figure 3.10. Micrographs of INC693-FeP1150 (Inconel 693, 7 days at 1150°C) (cont'd).

Figure 3.11. Cr concentration profile in coupon INC693-FeP1150 (Inconel 693 in FeP glass at 1150ºC for 7 days). Cr depletion is based on the SEM X-ray line scan into the coupon near the half-down area. Point analyses were done and are overlaid on the curve to calibrate concentration. The Cr depletion depth is about 300 μm.

a) Coupon cross section.

b) Detail of grain boundary attack region.
1, 2, 3, 4, 5 are all Al_2O_3

Figure 3.12. Micrographs of INC690-FeP1050-2 (Inconel 690, 14 days at 1050°C).
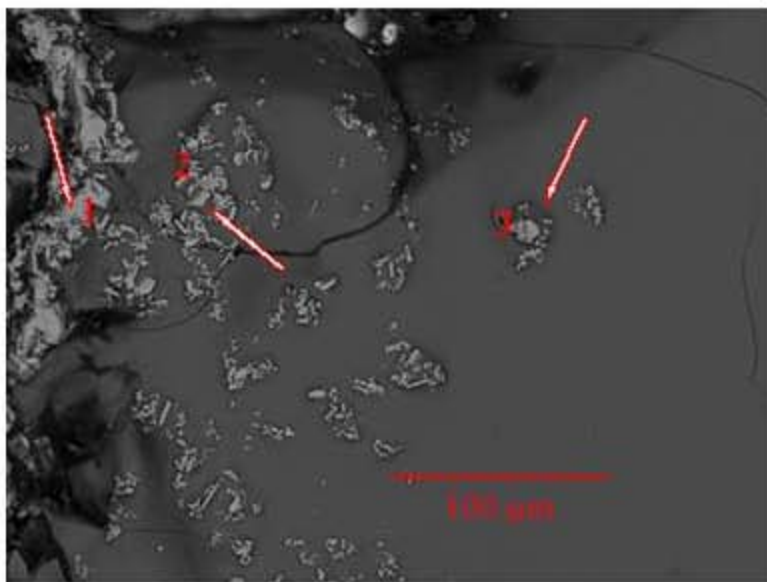
c) Corrosion products in scale
1: Cr_2O_3 containing a little Fe, Al, and a trace of Si, 2, 3: Fe-Cr-Al spinel
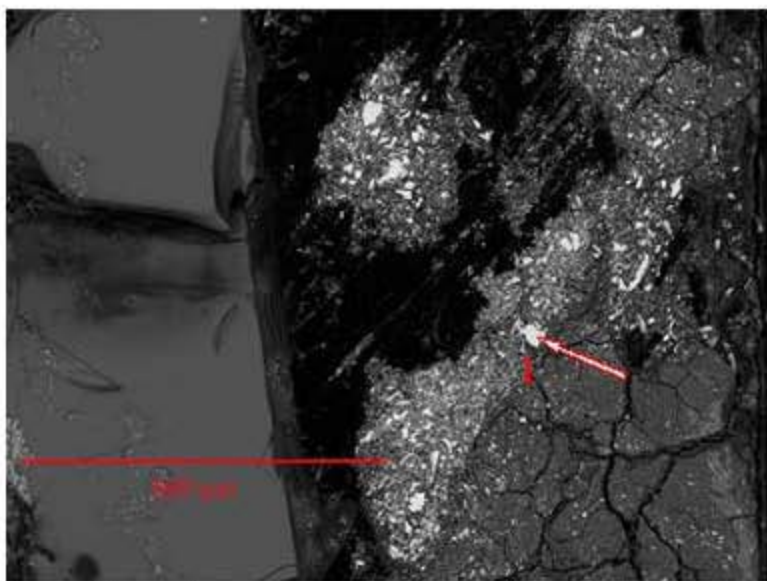
d) Inconel in scale
1: Inconel 690 metal particle

Figure 3.12. Micrographs of INC690-FeP1050-2 (Inconel 690, 14 days at 1050ºC) (cont'd).
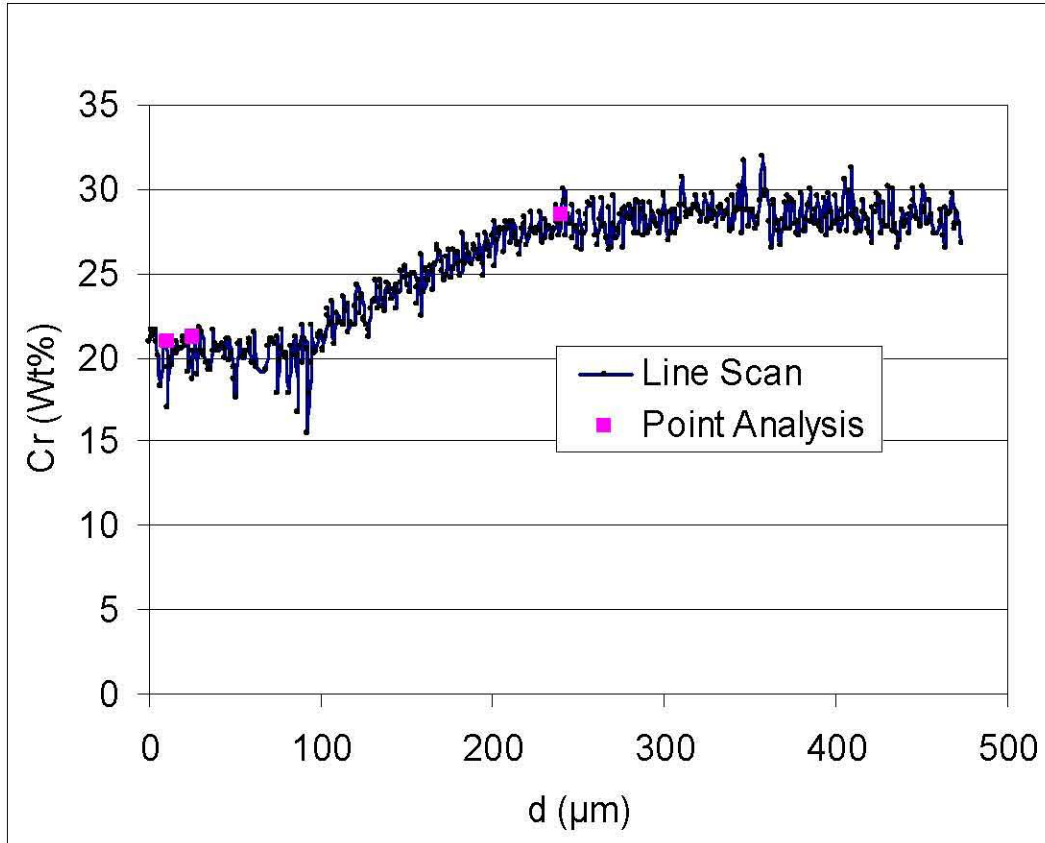
Figure 3.13. Cr concentration profile in coupon INC690-FeP1050-2 (Inconel 690 in FeP glass at 1050ºC for 14 days). Cr depletion is based on the SEM X-ray line scan into the coupon near the half-down area. Point analyses were done and are overlaid on the curve to calibrate concentration. The Cr depletion depth is about 250 μm.

a) Coupon surface near half-down area
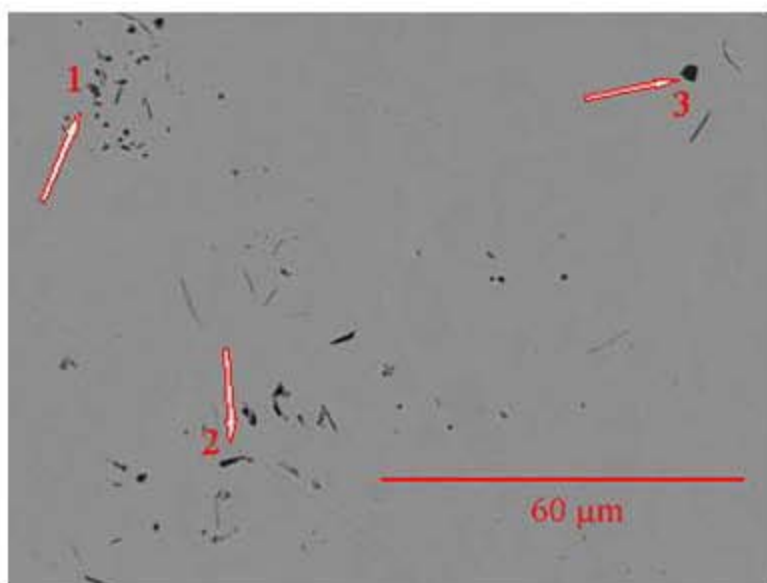
b) Detail of grain boundary attack
Phases 1, 2 and 3 are all Al_2O_3

Figure 3.14. Micrographs of INC693-FeP1050-2 (Inconel 693, 14 days at 1050°C).
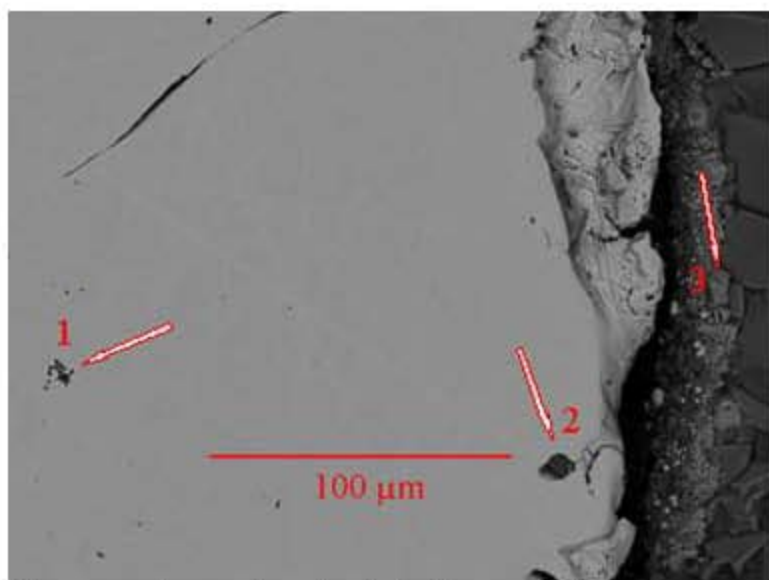
c) Coupon surface and scale originally attached to coupon.
1: Al_2O_3 and MgO, probably $MgAl_2O_4$ spinel, 2: Al_2O_3, 3: Fe-Cr-Al spinel. The Mg in phase 1 probably came from a contaminant in the original Inconel.

Figure 3.14. Micrographs of INC693-FeP1050-2 (Inconel 693, 14 days at 1050°C) (cont'd).
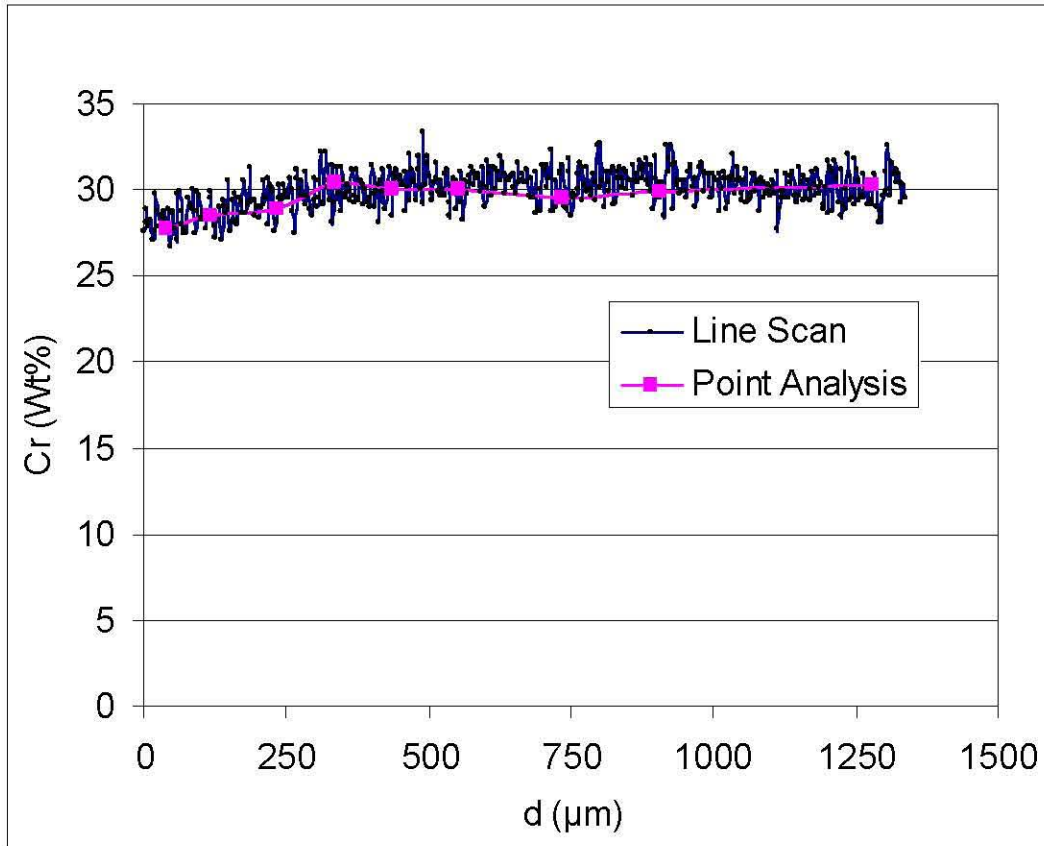
Figure 3.15. Cr concentration profile in coupon INC693-FeP1050-2 (Inconel 693 in FeP glass at 1050°C for 14 days). Cr depletion is based on the SEM X-ray line scan into the coupon near the half-down area. Point analyses were done and are overlaid on the curve to calibrate concentration. Depletion depth for Cr is about 325 μm.
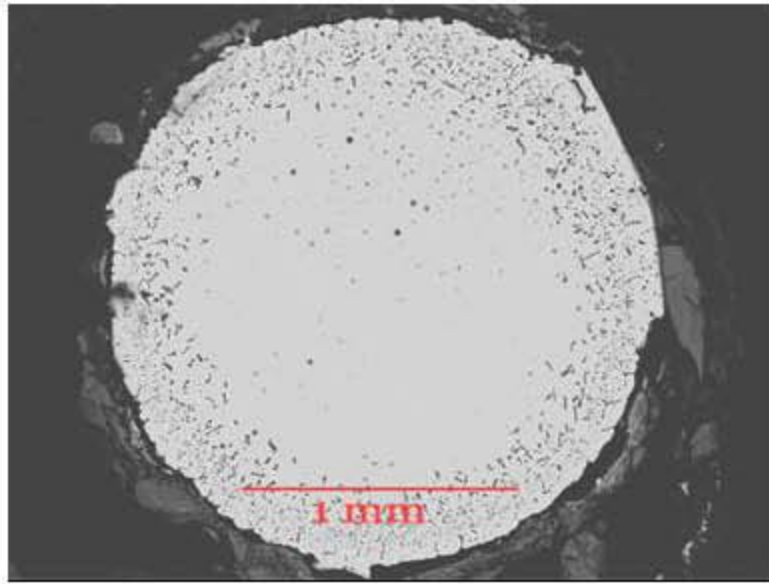
a) SEM micrograph of full cross section at 1.5 mm from the pin tip
The surrounding glass and scale are present.
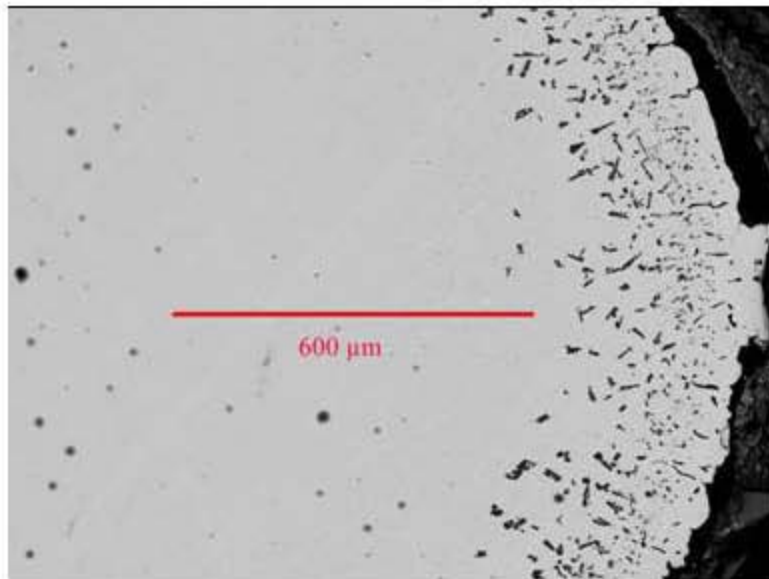
b) Detailed SEM micrograph of center to edge of coupon.
The somewhat fuzzy, small (5-20 µm) black spots toward the center are not corrosion
features, but carbon contamination. X-ray line scan to determine composition profiles
was done in this area.

Figure 3.16. Micrographs of INC693EC-1050-A (Inconel 693 pin in FeP glass at 1050°C for 3 days at a current density of 10 A/inch^2; Section 1.5 mm from tip).
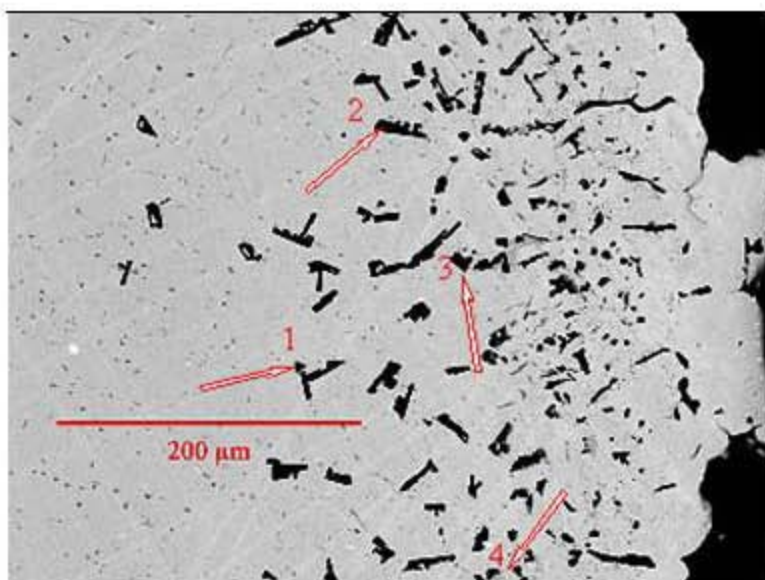
c) Edge region of the 1.5 mm section of the coupon

1: Ti-Zr-Nb nitride phase, 2, 3: Aluminum nitride phase, 4: Cr-Ni phosphide phase (very light grey and difficult to see in the micrograph; present only in band from 50 to 100 µm beneath the coupon surface.)

Element	N*	O*	Al	P	Ti	Cr	Ni	Zr	Nb	Ag
Arrow 1	0.46	-	-	-	1.0	0.02	-	0.05	0.04	-
Arrow 2	0.43	-	1.0	-	-	-	-	-	-	-
Arrow 3	0.38	0.08	1.0	-	-	0.01	0.01	-	-	0.004
Arrow 4	-	-	-	0.04	-	1.0	0.57	-	-	-

Entries are atomic ratios referenced to most abundant element taken as 1.

*These are light elements in a heavy matrix and so the ratios are subject to high uncertainty since they were obtained by standardless EDS analysis.

Figure 3.16. Micrographs of INC693EC-1050-A (Inconel 693 pin in FeP glass at 1050°C for 3 days at a current density of 10 A/inch^2; Section 1.5 mm from tip) (cont'd).
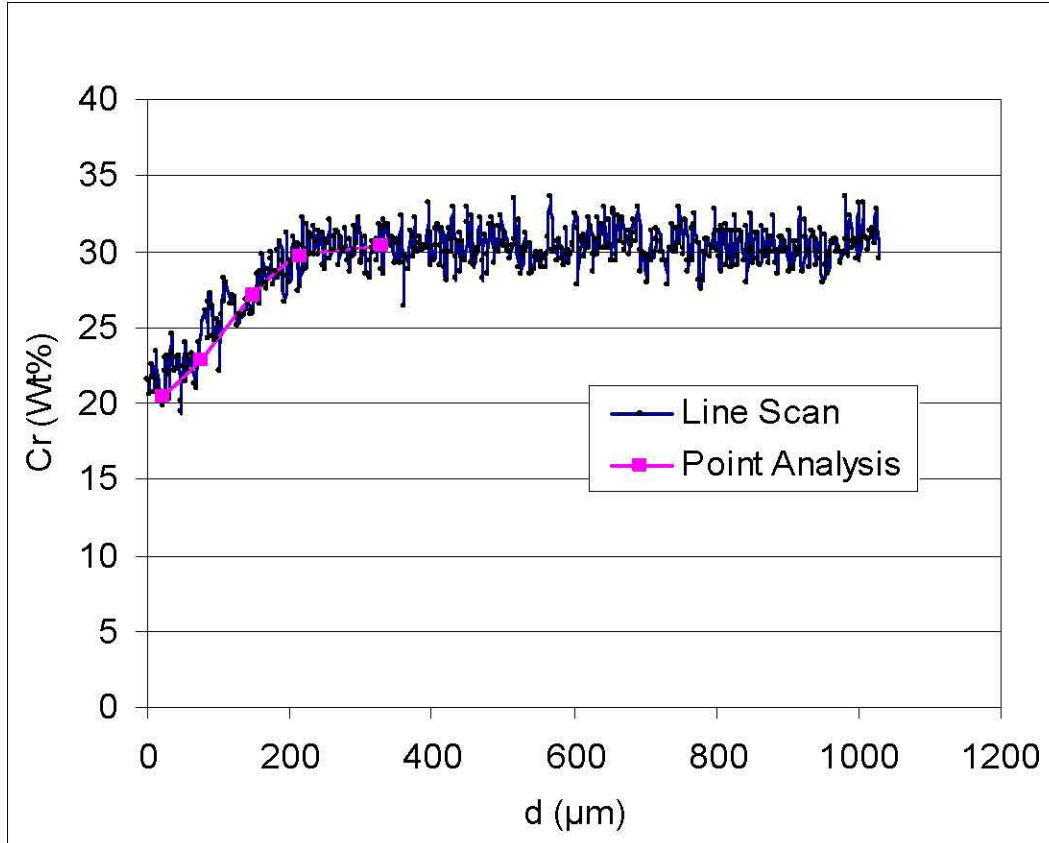
Figure 3.17. Cr concentration profile in coupon INC693EC-1050-A (Inconel 693 pin, immersed in FeP glass at 1050ºC for 3 days at a current density of 10 A/ in^2; sectioned 1.5 mm from tip). Cr depletion is based on the SEM X-ray line scan into the sectioned coupon. Point analyses were done and are overlaid on the curve to calibrate concentration. The Cr depletion depth is about 200 μm.
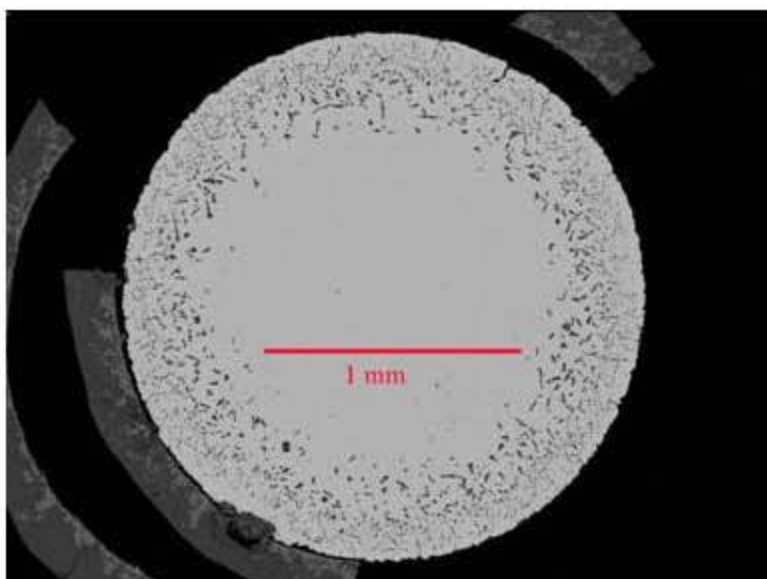
a) SEM micrograph of full cross section at 5.0 mm from the pin tip
The surrounding glass and scale are present, but mostly detached.
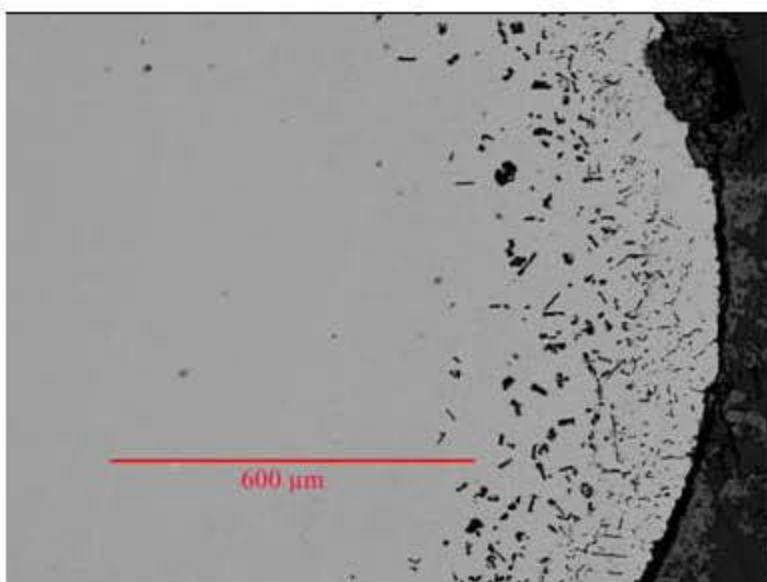
b) More detailed SEM micrograph of center to edge of coupon
X-ray line scan to determine composition profiles was done in this area.

Figure 3.18. Micrographs of INC693EC-1050-B (Inconel 693 pin in FeP glass at 1050°C for 3 days at a current density of 10 A/inch^2; Section 5.0 mm from tip).
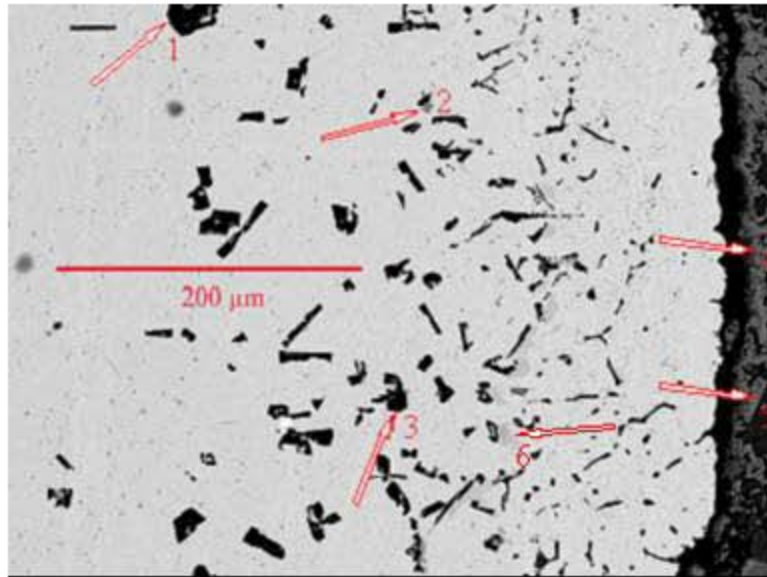
c)   Edge region of the 5.0 mm section of the coupon

1 and 3 are aluminum nitride phase, 4 and 5 are Cr_2O_3 containing 5 to 8 at% Fe, 6 is Cr-Ni phosphide phase (very light grey).

Element	N*	Al	P	Ti	Cr	Ni	Zr	Nb
Arrow 1	0.49	1.0	-	--	-	-	-	-
Arrow 2	0.19		-	1.0	0.02	0.02	0.07	0.05
Arrow 3	0.45	1.0	-	-	-	-	-	-
Arrow 6	-	-	0.02	-	1.0	0.59	0.01	0.01

Entries are atomic ratios referenced to most abundant element taken as 1.

*These are light elements in a heavy matrix and so the ratios are subject to high uncertainty since they were obtained by standardless EDS analysis.

Figure 3.18. Micrographs of INC693EC-1050-B (Inconel 693 pin in FeP glass at 1050°C for 3 days at a current density of 10 A/inch² ; Section 5.0 mm from tip) (cont'd).
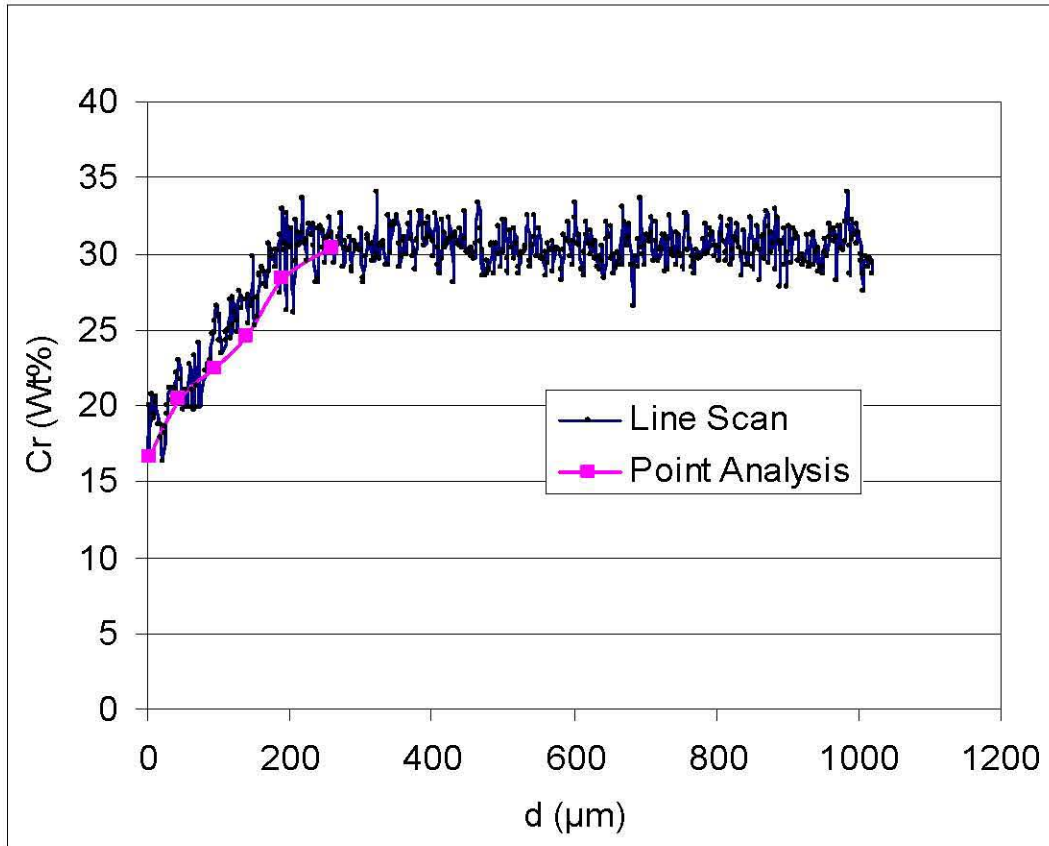
Figure 3.19. Cr concentration profile in coupon INC693EC-1050-B (Inconel 693 pin, immersed in FeP glass at 1050°C for 3 days at a current density of 10 A/ in^2; sectioned 5.0 mm from pin tip). Cr depletion is based on the SEM X-ray line scan into the sectioned coupon. Point analyses were done and are overlaid on the curve to calibrate concentration. The Cr depletion depth is about 220 μm.
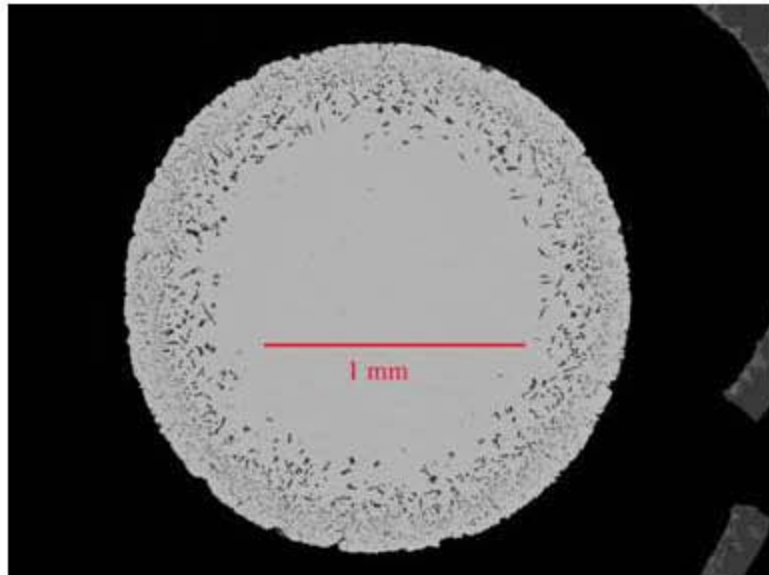
a) SEM micrograph showing 9 mm cross section.
Some detached surrounding glass and scale are visible at the right.
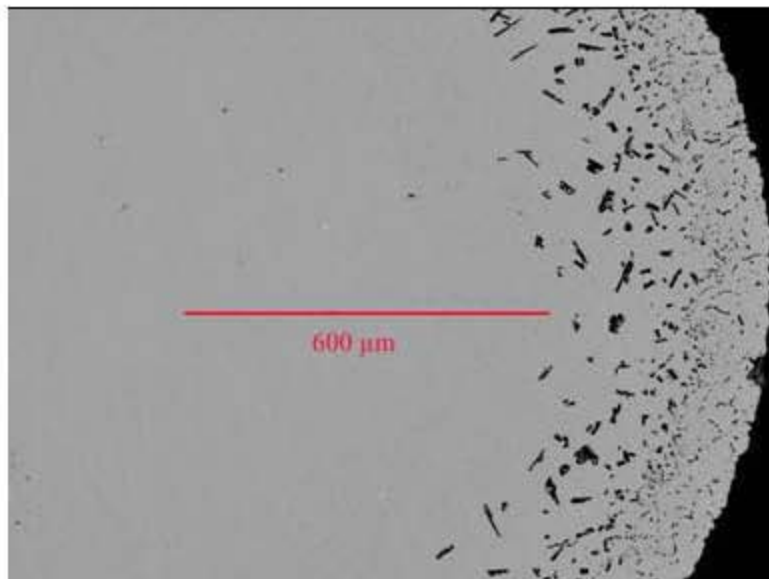
b) More detailed SEM micrograph of center to edge of coupon.
X-ray line scan to determine composition profiles was done in this area.

Figure 3.20. Micrographs of INC693EC-1050-C (Inconel 693 pin in FeP glass at 1050°C for 3 days at a current density of 10 A/inch^2; Section 9.0 mm from tip).
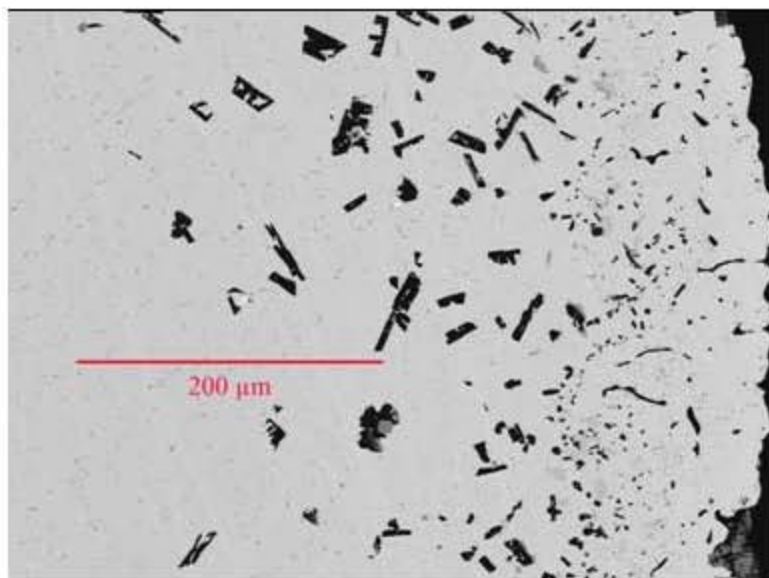
c) Edge region of the 9.0 mm section of the coupon

Figure 3.20. Micrographs of INC693EC-1050-C (Inconel 693 pin in FeP glass at 1050°C for 3 days at a current density of 10 A/inch² ; Section 9.0 mm from tip) (cont'd).
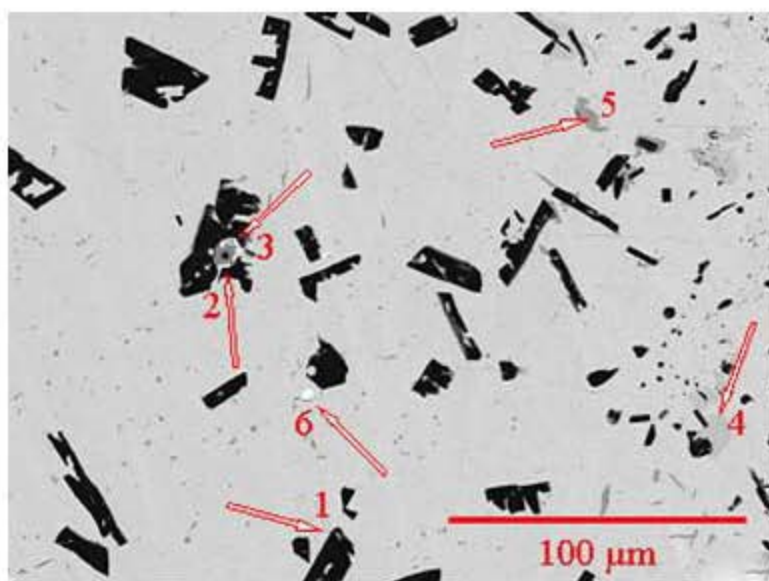
d) Edge region showing locations that were analyzed

Element	N*	O*	Al	P	Ti	Cr	Fe	Ni	Zr	Nb	Feature Color
Arrow 1	0.47	0.05	1.00	-	-	-	-	0.39	-	-	Black
Arrow 2	0.28	-	-	-	1.00	-	-	-	0.06	0.05	Dark Grey
Arrow 3	-	-	-	-	0.26	0.17		0.24	1.00	-	White
Arrow 4	-	-	-	0.05	-	1.00	0.03	0.57	-	-	Medium Grey
Arrow 5	0.13	-	-	-	-	1.00	-	0.03	-	-	Dark Grey
Arrow 6	-	-	-	-	0.26	0.27	-	0.39	1.00	0.41	White

Entries are atomic ratios referenced to most abundant element taken as 1.

*These are light elements in a heavy matrix and so the ratios are subject to high uncertainty since they were obtained by standardless EDS analysis.

Figure 3.20. Micrographs of INC693EC-1050-C (Inconel 693 pin in FeP glass at 1050°C for 3 days at a current density of 10 A/inch^2; Section 9.0 mm from tip) (cont'd).
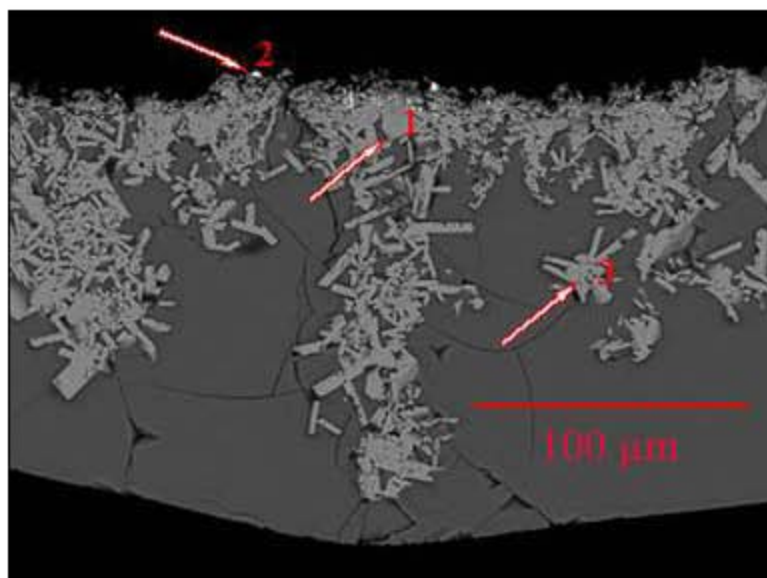
e)   Detached section of coupon scale

1: Cr_2O_3, 2: (White spot) Inconel corrosion residue, 3: Fe-Cr-Al spinel (chromite, $FeCr_2O_4$ containing some Al)

Element	O*	Al	Cr	Fe	Ni
Arrow #1	49.9	-	46.6	3.5	-
Arrow #2**	11.4	-	20.3	4.6	63.7
Arrow #3	48.4	1.4	35.0	15.2	-

All results are in atom%

*Standardless EDS analysis value; high uncertainty for light element in heavy matrix.
**Because of over-sampling by electron beam, presence of O is questionable in this phase, and other element values are subject to high uncertainty.

Figure 3.20. Micrographs of INC693EC-1050-C (Inconel 693 pin in FeP glass at 1050°C for 3 days at a current density of 10 A/inch^2; Section 9.0 mm from tip) (cont'd).
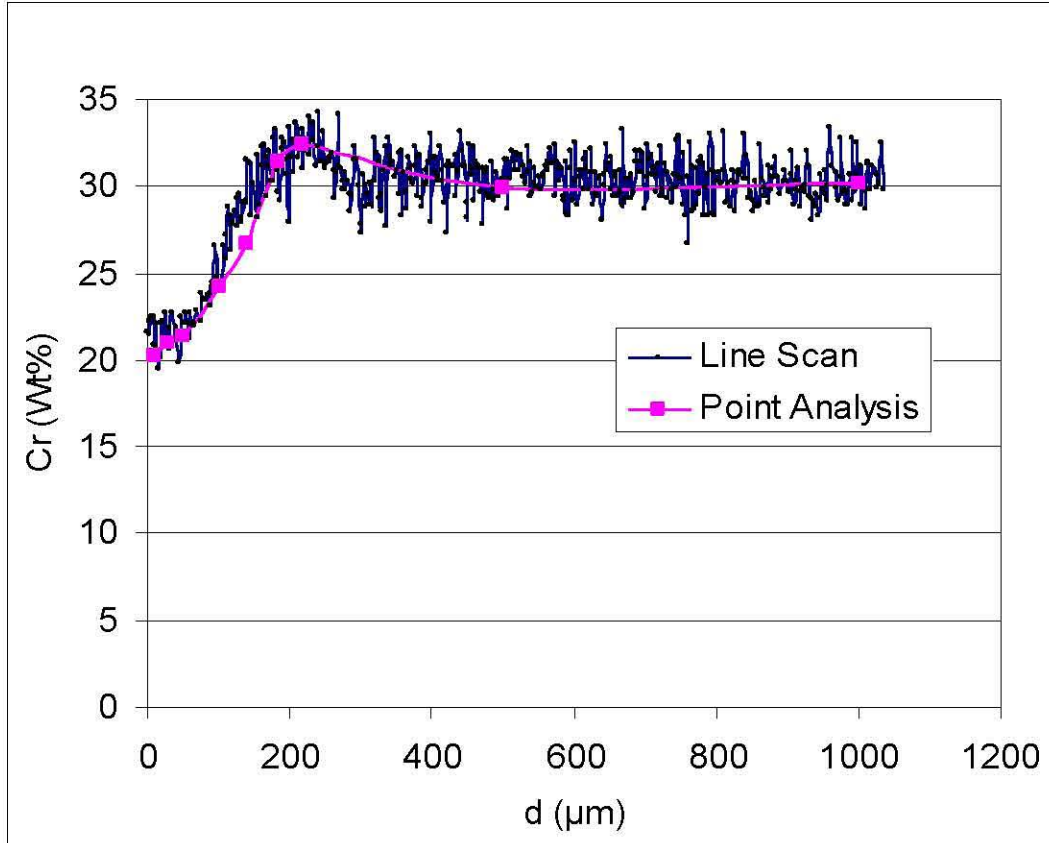
Figure 3.21. Cr concentration profile in coupon INC693EC-1050-C (Inconel 693 pin immersed in FeP glass at 1050ºC for 3 days at a current density of 10 A/ in^2; sectioned 9.0 mm from pin tip). Cr depletion is based on the SEM X-ray line scan into the sectioned coupon. Point analyses were done and are overlaid on the curve to calibrate concentration. The Cr depletion depth is about 180 μm.
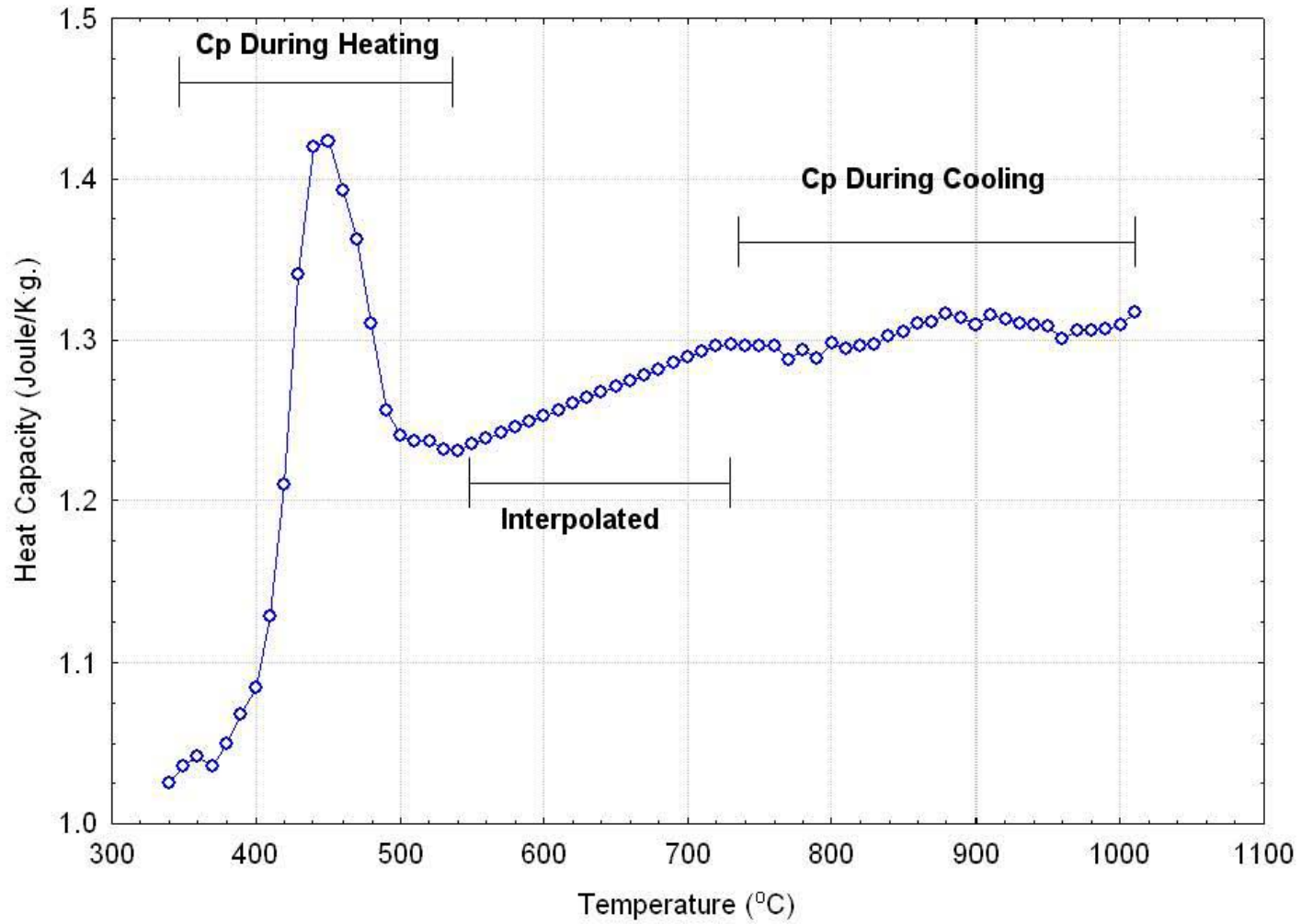
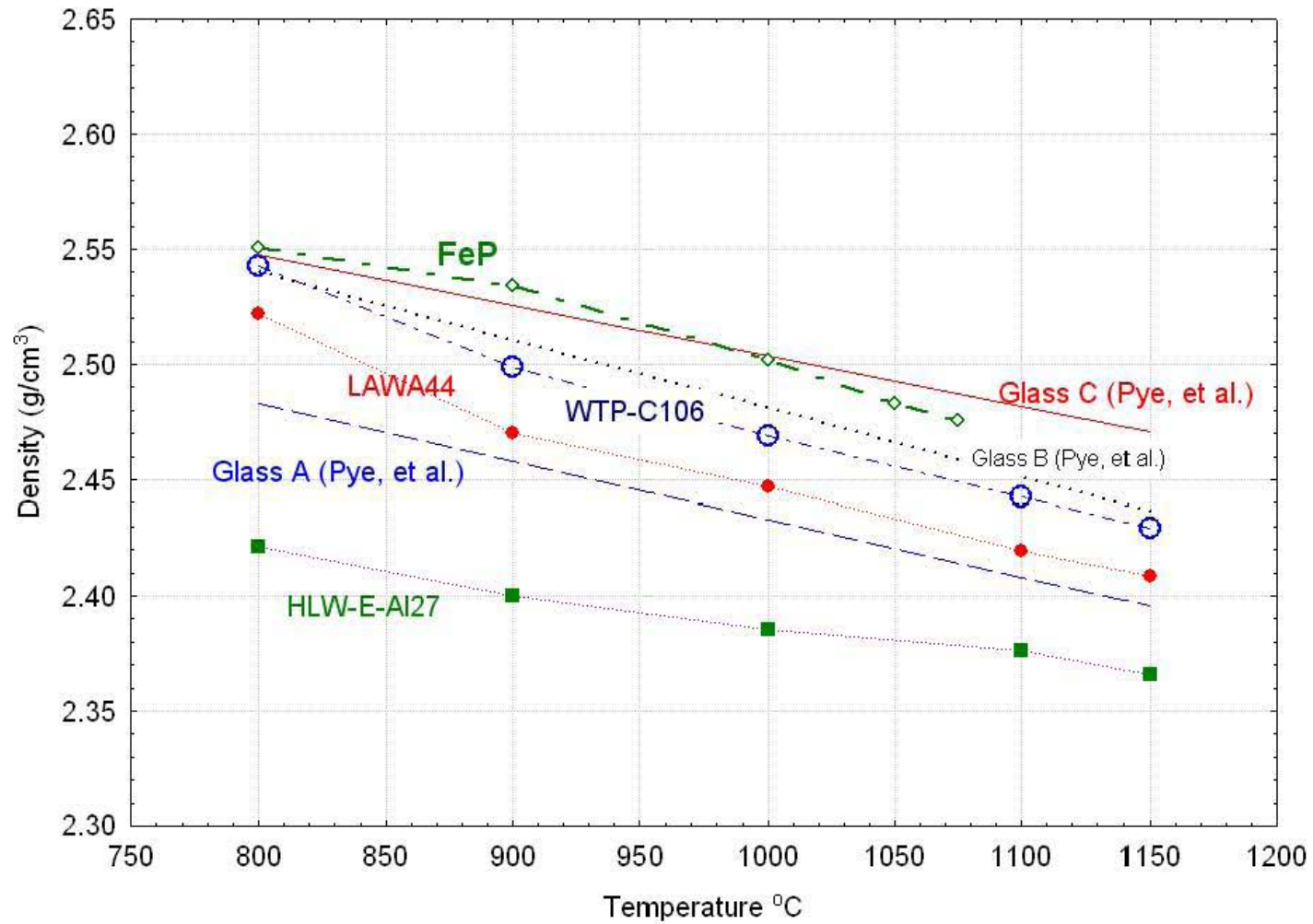**Figure 4.1.   Heat capacity of FeP glass.**

Figure 4.2. Density of FeP glass along with density data for four simulated WTP waste glass melts and three simulated waste glass melts from regression equations provided by Pye et al. [17].
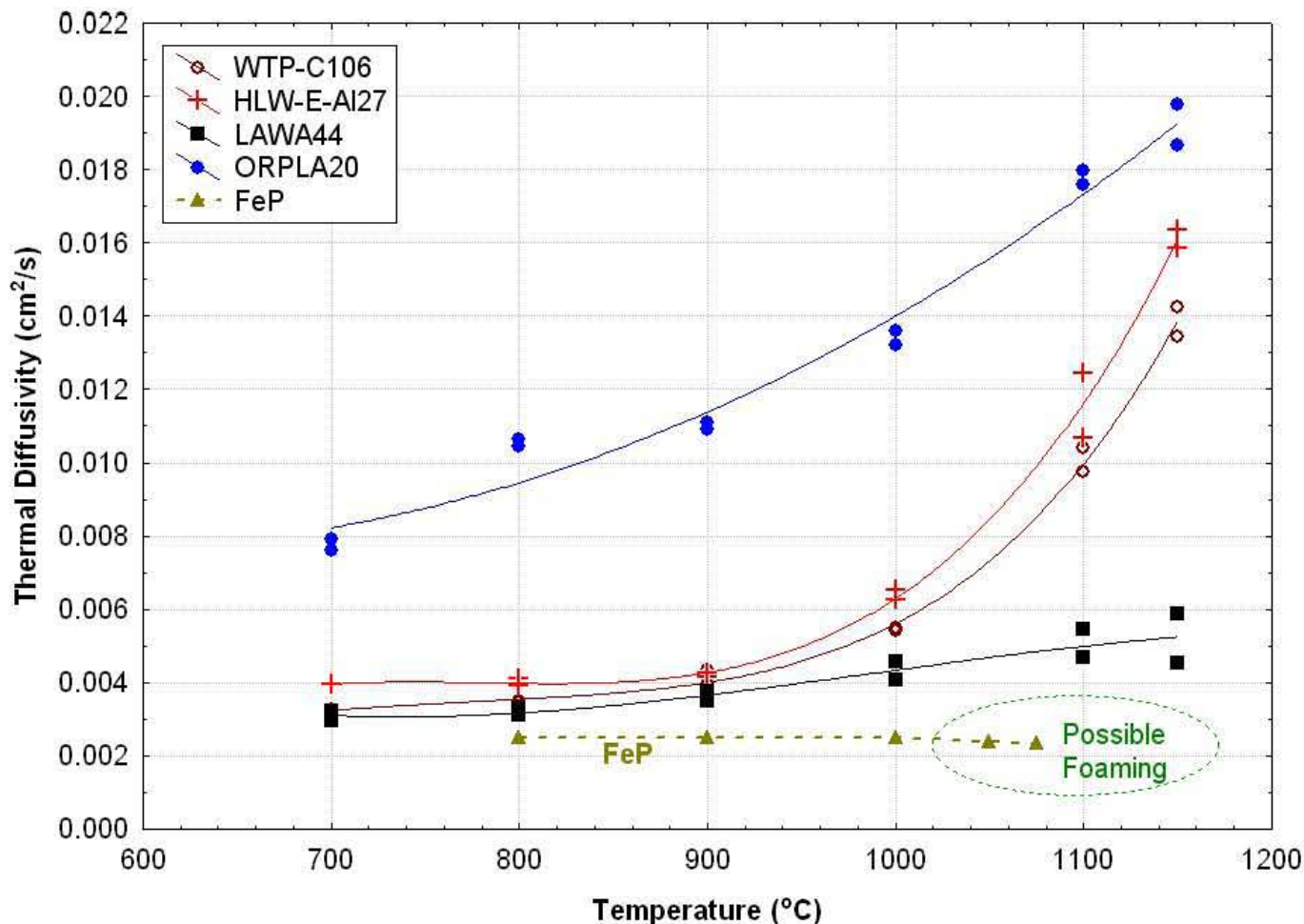
Figure 4.3. Thermal Diffusivity of FeP glass and four simulated WTP waste glass melts. Multiple points for a melt sample at a given temperature are from separate experiments using heat waves of different periods. Curves are polynomial fits.
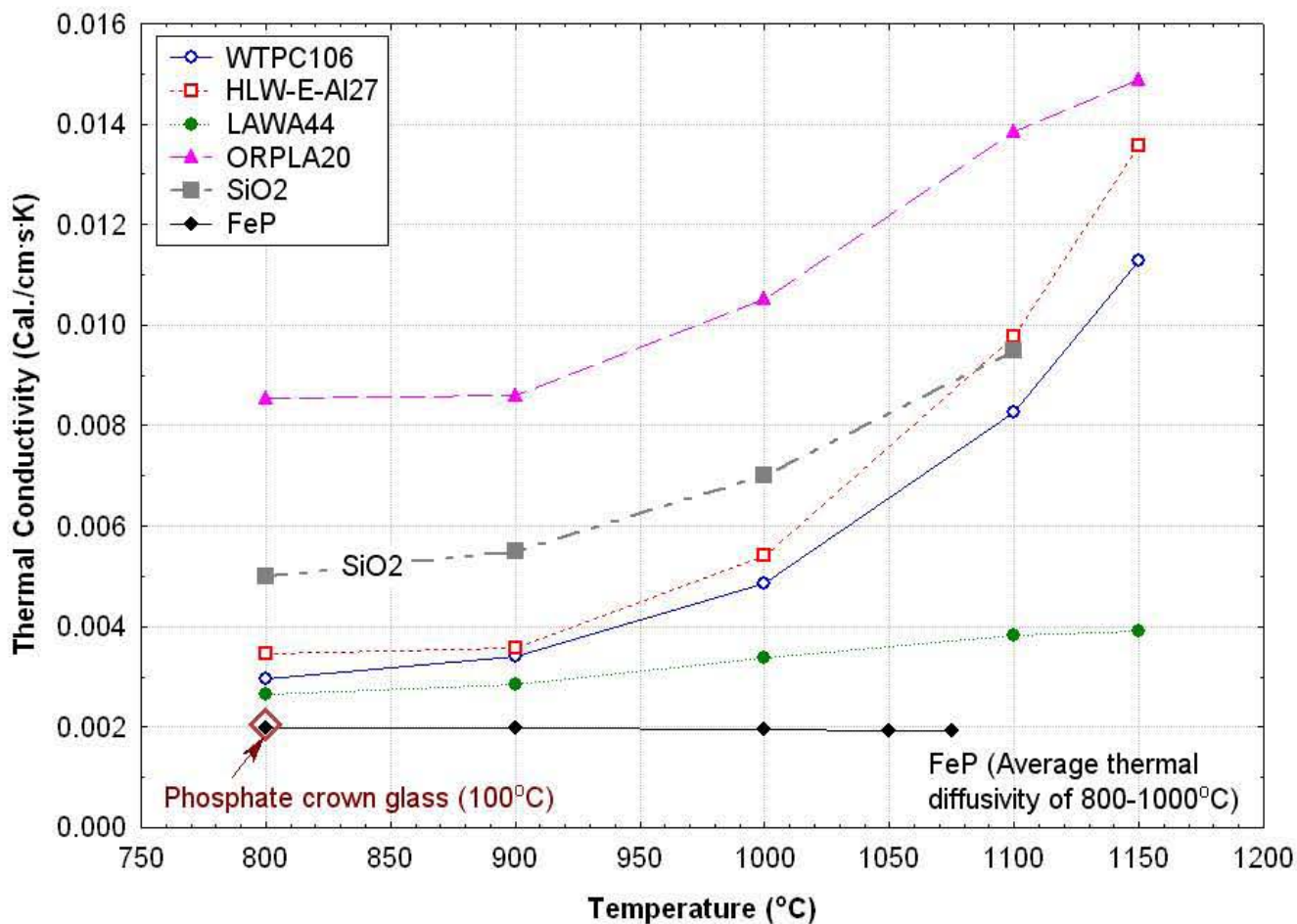
Figure 4.4. Thermal conductivity of FeP glass calculated from data for specific heat, density, and thermal diffusivity. Thermal conductivity values for four simulated WTP waste glasses and SiO₂ glass are included for comparison.